

DTIC FILE COPY

AFOSR-TR- 88 - 0609

2

THE USE OF LASER-POWERED HOMOGENEOUS PYROLYSIS TO DETERMINE THE INITIAL STEPS IN THE HOMOGENEOUS GAS-PHASE DECOMPOSITION OF CYCLIC NITRAMINES

April 1988

Final Technical Report
Covering the period 1 January 1985 thru 31 December 1987

By: Donald F. McMillen, Paul H. Stewart,
S. Esther Nigenda, Jay B. Jeffries,
Jean-Michel Zellweger, Roberta P. Saxon,
and David M. Golden

Prepared for:

AIR FORCE OFFICE OF SCIENTIFIC RESEARCH
Directorate of Chemical Sciences (NC)
Building 410
Bolling Air Force Base
Washington, DC 20332-6448

Attention: Major Larry P. Davis, Program Manager

Contract No. F49620-85-K-0006
SRI Project PYU-8232
CK 88-22

DTIC
ELECTE
JUN 29 1988
S H D

SRI International
333 Ravenswood Avenue
Menlo Park, California 94025-3493
(415) 326-6200
TWX: 910-373-2046
Telex: 334486

AIR FORCE OFFICE OF SCIENTIFIC RESEARCH (AFSC)
NOT FOR DISTRIBUTION TO DTIC
Approved for release by AFSC/AFI 150-12.
Distribution is limited to AFSC/AFI 150-12.
SRI International
Director, Technical Information Division



Approved for public release;
distribution unlimited.

88 6 29 015

SRI International



THE USE OF LASER-POWERED HOMOGENEOUS PYROLYSIS TO DETERMINE THE INITIAL STEPS IN THE HOMOGENEOUS GAS-PHASE DECOMPOSITION OF CYCLIC NITRAMINES

April 1988

Final Technical Report
Covering the period 1 January 1985 thru 31 December 1987

By: Donald F. McMillen, Paul H. Stewart,
S. Esther Nigenda, Jay B. Jeffries,
Jean-Michel Zellweger, Roberta P. Saxon,
and David M. Golden

Prepared for:

AIR FORCE OFFICE OF SCIENTIFIC RESEARCH
Directorate of Chemical Sciences (NC)
Building 410
Bolling Air Force Base
Washington, DC 20332-6448

Attention: Major Larry P. Davis, Program Manager

Contract No. F49620-85-K-10006
SRI Project PYU-8232
CK 88-22

Approved by:

D. C. Lorents, Director
Chemical Physics Laboratory

G. R. Abrahamson
Vice President
Physical Sciences Division

UNCLASSIFIED

SECURITY CLASSIFICATION OF THIS PAGE

REPORT DOCUMENTATION PAGE

1a. REPORT SECURITY CLASSIFICATION UNCLASSIFIED		1b. RESTRICTIVE MARKINGS N/A	
2a. SECURITY CLASSIFICATION AUTHORITY N/A		3. DISTRIBUTION/AVAILABILITY OF REPORT Approved for DTIC Release; Distribution Unlimited.	
2b. DECLASSIFICATION/DOWNGRADING SCHEDULE N/A			
4. PERFORMING ORGANIZATION REPORT NUMBER(S) PYU-8232		5. MONITORING ORGANIZATION REPORT NUMBER(S) AFOSR-TR- 88-0609	
5a. NAME OF PERFORMING ORGANIZATION SRI International	6b. OFFICE SYMBOL (if applicable)	7a. NAME OF MONITORING ORGANIZATION Air Force Office of Scientific Research	
6c. ADDRESS (City, State, and ZIP Code) 333 Ravenswood Avenue Menlo Park, CA 94025		7b. ADDRESS (City, State, and ZIP Code) Directorate of Chemical Sciences (NC) Bldg. 410, Bolling Air Force Base Washington, DC 20332-6448	
8a. NAME OF FUNDING/SPONSORING ORGANIZATION AFOSR	8b. OFFICE SYMBOL (if applicable) NIC	9. PROCUREMENT INSTRUMENT IDENTIFICATION NUMBER F49620-85-K-0006	
9c. ADDRESS (City, State, and ZIP Code) Building 410 Bolling AFB DC 20332-6448		10. SOURCE OF FUNDING NUMBERS	
	PROGRAM ELEMENT NO. 61-02F	PROJECT NO. 2303	TASK NO. B1
11. TITLE (Include Security Classification) The Use of Laser-Powered Homogeneous Pyrolysis to Determine the Initial Steps in the Homogeneous Gas-Phase Decomposition of Cyclic Nitramines			
12. PERSONAL AUTHOR(S) McMillen, Donald F., Stewart, Paul H., Nigenda, S. Esther, Jeffries, Jay B., Zellwegger, Jean-Michel, Saxon, Roberta P., Golden, David M.			
13a. TYPE OF REPORT Final	13b. TIME COVERED FROM 850101 TO 871231	14. DATE OF REPORT (Year, Month, Day) 880428	15. PAGE COUNT 107
16. SUPPLEMENTARY NOTATION			
17. COSATI CODES		18. SUBJECT TERMS (Continue on reverse if necessary and identify by block number) SYNTHESIS (CHEMISTRY) gas phase decomposition, dimethylnitrosamine, cyclic nitramines, dimethylnitramine, JIS	
FIELD 07	GROUP 04		
19. ABSTRACT (Continue on reverse if necessary and identify by block number) As a prototype for more complex nitramines, the gas-phase decomposition of dimethylnitramine has been studied experimentally in two different laser-pyrolysis systems and theoretically using <u>ab initio</u> quantum mechanical calculations. Our studies, unlike those reported in the literature, indicate that a nitro-nitrite rearrangement pathway is competitive with the expected (and previously invoked) N-NO ₂ bond scission. This rearrangement pathway has been obscure because it can lead to some of the same products as are yielded by the bond scission route. The principal evidence for nitro-nitrite rearrangement is (1) Arrhenius parameters for			
20. DISTRIBUTION/AVAILABILITY OF ABSTRACT <input checked="" type="checkbox"/> UNCLASSIFIED/UNLIMITED <input type="checkbox"/> SAME AS RPT. <input type="checkbox"/> DTIC USERS		21. ABSTRACT SECURITY CLASSIFICATION Unclassified	
22a. NAME OF RESPONSIBLE INDIVIDUAL Major Larry P. Davis		22b. TELEPHONE (Include Area Code) (202) 767-4963	22c. OFFICE SYMBOL NIC

DD FORM 1473, 84 MAR

83 APR edition may be used until exhausted.
All other editions are obsolete.

SECURITY CLASSIFICATION OF THIS PAGE

UNCLASSIFIED

19. ABSTRACT

decomposition ($\log k/s^{-1} = 13.5 + 0.6 - [37.4 + 2.5]/2.3RT$) that are two orders of magnitude too low to be consistent with simple N-NO₂ bond scission as the sole rate-determining step; (2) molecular-beam, mass-spectrometrically-sampled laser pyrolysis studies that show direct detection of NO and the nitroxyl radical (CH₃)₂NNO· on a time scale too short to allow for the production of these substances in secondary bimolecular reactions; and (3) ab initio calculations that find a rearrangement pathway at slightly lower energy than that of simple bond scission. These results suggest that such rearrangement pathways may be a common feature of nitramine decomposition, as other studies have recently shown them to be for C-NO₂ compounds. In the course of repeated synthesis of dimethylnitramine, we also developed a new method of synthesis via the nitrodephosphorylation of phosphoramides, which is very convenient for certain nitramines.

Y. ...

CONTENTS

INTRODUCTION.....1

LASER PYROLYSIS OF DIMETHYLNITRAMINE AND DIMETHYLNITROSAMINE.....3

 GC/MS-Monitored Laser Pyrolysis.....4

 Molecular-Beam, Mass-Spectrometrically-Monitored Laser Pyrolysis.....4

AB INITIO QUANTUM MECHANICAL CALCULATIONS.....6

NITRAMINE SYNTHESSES.....7

CONCLUSIONS.....8

REFERENCES.....9

APPENDICES

 A. THERMAL DECOMPOSITION OF DIMETHYLNITRAMINE AND
 DIMETHYLNITROSAMINE BY PULSED LASER PYROLYSIS.....A-1

 B. MOLECULAR-BEAM SAMPLED LASER PYROLYSIS OF
 DIMETHYLNITRAMINE.....B-1

 C. THEORETICAL STUDY OF NITRO-NITRITE REARRANGEMENT OF NH_2NO_2C-1

 D. SYNTHESIS OF N,N-DIMETHYLNITRAMINE BY NITRODEPHOSPHORYLATION
 OF HEXAMETHYLPHOSPHORAMIDE.....D-1



Accession For	
NTIS GRA&I	<input checked="" type="checkbox"/>
DTIC TAB	<input type="checkbox"/>
Unannounced	<input type="checkbox"/>
Justification	
By	
Distribution/	
Availability Codes	
Dist	Avail and/or Special
A-1	

INTRODUCTION

The principal objective of this project has been to identify and determine the thermal rate parameters for the initial and/or rate-limiting steps in the gas-phase decomposition of nitramines. In support of this goal, which has also received funding from the Army Research Office (ARO), we have applied three different approaches. Experimentally, we have used two laser pyrolysis systems to study the initial and secondary reactions in the decomposition of dimethylnitramine. The theoretical effort has involved the use of ab initio quantum mechanical calculations to help determine the extent to which nitro-nitrite rearrangement is a competitive pathway in the decomposition of nitramines. The results of each of these approaches are summarized in this section and presented in detail in Appendices A through D, each of which is a manuscript submitted, or to be submitted, for publication.

As an important class of energetic materials, nitramines have been the subject of numerous studies whose goals have been to elucidate various facets of the chemistry that determines whether a self-sustaining reaction is achieved and, in the case of propellant compositions, determines the rate of combustion. Inasmuch as attempts to modify the burn rates of nitramine propellants have met with only very modest success, and inasmuch as the high pressure-dependence of HMX combustion rate aggravates a tendency towards instability and deflagration-to-detonation phenomena, achieving a better understanding of nitramine chemistry could have substantial practical impact. However, the chemical details of nitramine decomposition, like those for other energetic materials, have been very difficult to ascertain. This is hardly surprising, because in substances that decompose by one or more rate-limiting initial endothermic steps followed by a sequence of highly exothermic and very rapid steps, the nature of the rate-limiting steps themselves tends to be obscured. Characterizing nitramine decomposition is particularly difficult not only because secondary bimolecular reactions of radicals with NO_2 are particularly fast but also because the aliphatic radicals formed from

the carbon-nitrogen skeleton have a wider range of possible reactions than, for example, the typical aromatic radical produced in nitroaromatic decomposition.

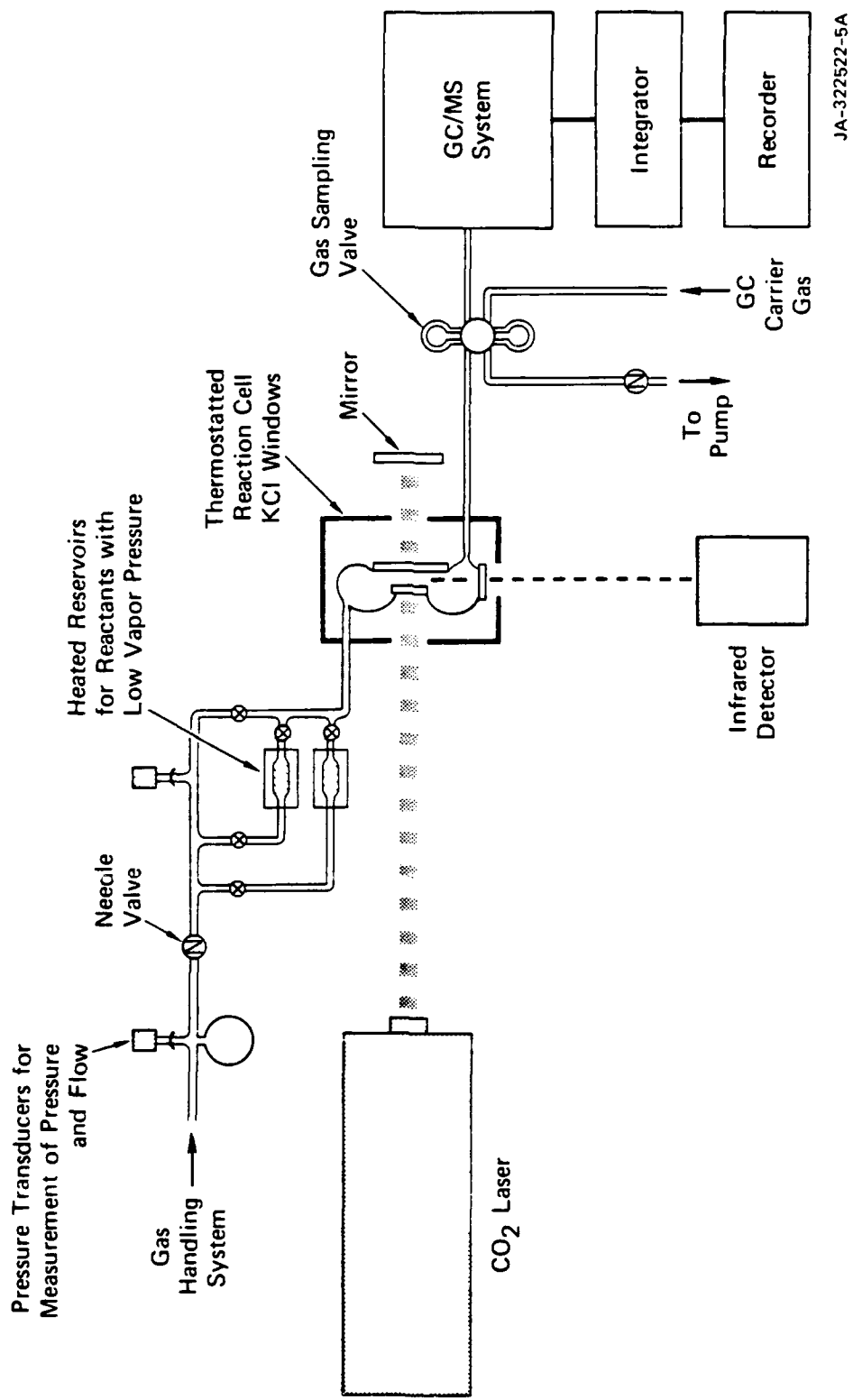
Dimethylnitramine (DMNA) decomposition is not exactly analogous to decomposition of the cyclic nitramines, which have several additional pathways potentially available.^{1,2} However, because previous research shows that understanding DMNA decomposition is difficult,³⁻⁹ we chose to study competition in the reaction pathways of DMNA before tackling RDX and HMX, which have more complex chemistry, lower vapor pressures, and higher reactivity.

The expedient commonly used in attempts to minimize the obscuring of rate-limiting steps by rapid secondary reactions is to perform the decomposition at much lower temperatures and/or much lower pressures (concentrations) than those involved during "normal" operation. Drastically different temperature and pressure conditions are likely to cause significant shifts in competing reactions and, therefore, leave undetermined the rate-limiting steps that are actually operative under practical conditions. In our research, we lowered the pressure but not the temperature and used very short reaction times.

LASER PYROLYSIS OF DIMETHYLNITRAMINE AND DIMETHYLNITROSAMINE

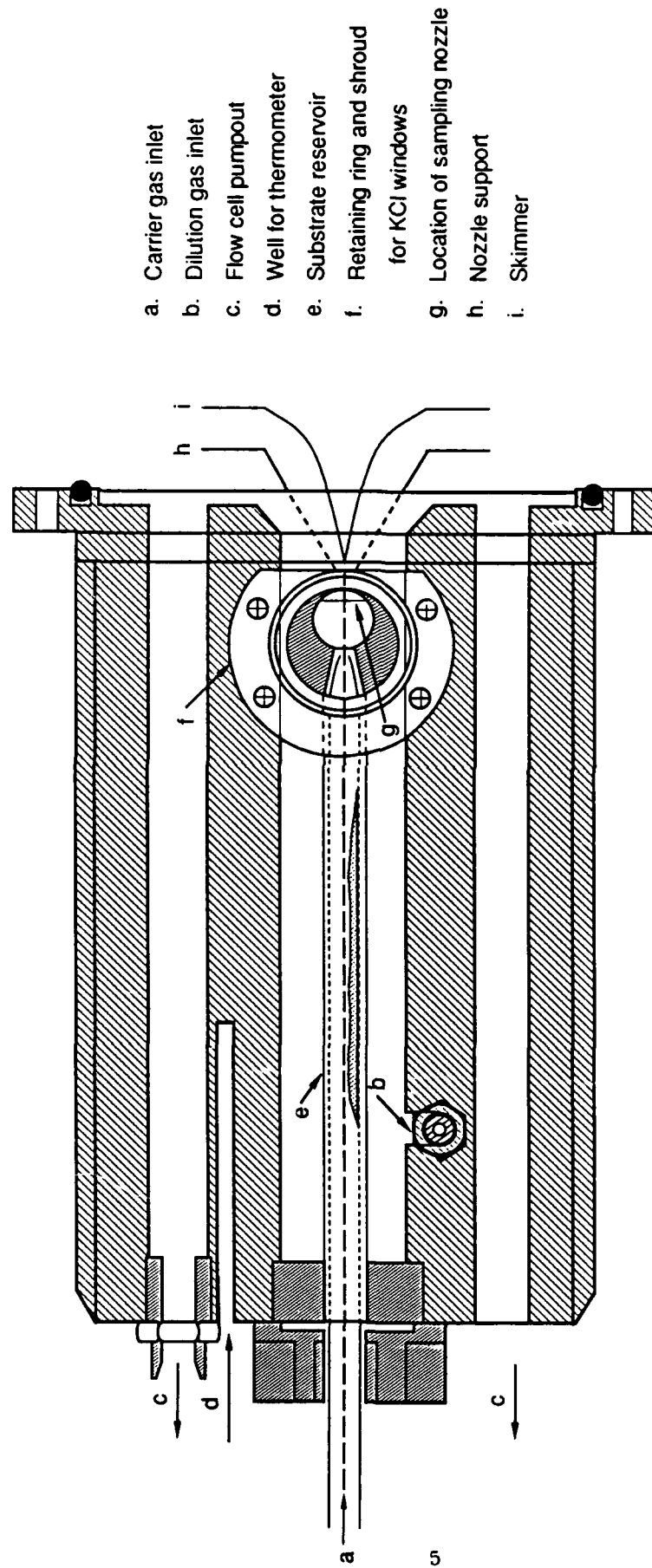
To help determine the rate-limiting step or steps at relevant temperatures, we chose an intermediate experimental course in which the pressure but not the temperature is significantly lowered and the reaction time is very short. A pulsed infrared laser is used to heat the substrate by heating an absorbing but unreactive gas (e.g., SF_6) that then transfers its kinetic energy by collision; in this way, the substrate is brought to high temperature (700-1200K) in 1-3 μs . Reaction then occurs in the 1 to 15 μs in which the acoustic expansion wave moves radially inward toward the center of the laser-heated region. By using different methods of sampling the product mixture, we can examine different extents of secondary reactions.

We have used two different techniques to determine products: One involves passing the contents of the cell shown in Figure 1 through an automatically operated gas-sampling valve, which periodically injects a sample into a GC/MS system. This provides a time-averaged mixture of products from the entire reaction zone and a reliable average temperature/reaction time from the simultaneously determined fractional decomposition of a temperature standard.¹⁰⁻¹² The second technique involves a separate apparatus (Figure 2) in which the laser-heated region is located immediately adjacent to the sampling nozzle of a molecular-beam mass spectrometric detection system. In this case, the gas mixture in the laser-heated region expands toward the nozzle, and the product mixture is frozen by the molecular-beam formation. The product mixture in the periphery of the laser-heated region has the least opportunity for secondary reaction, and that in the inner portions has progressively more opportunity. With both sampling techniques, the extent of secondary reaction can be varied by varying the substrate partial pressure, the extent of the initial reaction, and the presence of radical scavengers and radical traps. The presence of scavengers and traps has been particularly important in investigating DMNA, which, its apparent simplicity notwithstanding, has a number of initial and secondary reaction pathways open to it.



JA-322522-5A

Figure 1. Schematic of gas chromatographically monitored laser-powdered homogeneous pyrolysis flow system.



- a. Carrier gas inlet
- b. Dilution gas inlet
- c. Flow cell pumpout
- d. Well for thermometer
- e. Substrate reservoir
- f. Retaining ring and shroud for KCl windows
- g. Location of sampling nozzle
- h. Nozzle support
- i. Skimmer

JA-M-8232-6

Figure 2. Schematic drawing of the machined aluminum flow cell.

GC/MS-Monitored Laser Pyrolysis

DMNA was pyrolyzed over the temperature range 800 to 900K in a flow system using pulsed infrared laser heating. The major product under all conditions was dimethylnitrosamine (DMNO), with smaller amounts of N-methylmethyleimine and dimethylamine also produced when radical scavengers and traps were not both present. Arrhenius parameters for the decomposition were $\log k(s^{-1}) = 13.5 + 0.6 - (37.4 + 2.5)/2.3RT$. These parameters, which were produced under a wide range of conditions (different scavengers, different temperatures, and varying amounts of added NO as a trap for dimethylamino radicals), are not consistent with simple bond scission as the sole rate-limiting step. The principal product, DMNO, was studied under the same conditions; DMNO has no plausible decomposition pathways other than simple bond scission, and it decomposed with parameters appropriate to such a process, namely $\log k(s^{-1}) = 15.8 + 1.1 - (50.3 + 3.4)/2.3RT$. Moreover, the temperature dependence was evidently not distorted (as feared) by secondary reactions involving the highly reactive methyleneimine, which was the major product of DMNO decomposition, but a less important product of DMNA decomposition. The experimental products and temperature dependence can be reproduced via a mechanistic numerical model when N-NO₂ bond scission and nitro-nitrite rearrangement are competitive initial steps and the displacement of NO₂ from DMNA by NO is included as a low-temperature route to DMNO. Thus, these results lead us to conclude that DMNA decomposes not only by the expected simple bond scission reaction but also by an intramolecular nitro-nitrite rearrangement. Such reactions have been shown to occur in C-NO₂ systems¹³⁻¹⁵ but have not been previously reported in nitramines. These results are described in detail in Appendix A, a manuscript submitted to the Journal of Physical Chemistry.

Molecular-Beam Mass-Spectrometrically-Monitored Laser Pyrolysis

Because the products of an initial nitro-nitrite rearrangement can also result from a secondary bimolecular reaction in which the dimethylamino radical is oxidized by NO₂, and because the evidence summarized above for the intramolecular rearrangement, while extensive, is largely indirect, we used a second laser-pyrolysis system to examine directly the products of

dimethylnitramine decomposition. With this system (Figure 2), the product mixture in the laser-heated region expands directly into the nozzle of a molecular-beam sampling system and is detected by a quadrupole mass spectrometer. The initial products include not only dimethylamino radical and NO_2 but also comparable amounts of NO and various fragment ions of the nitroxyl radical $(\text{CH}_3)_2\text{NNO}^\cdot$. Although the bimolecular oxidation of radicals by NO_2 is known to be very rapid, the NO_2 partial pressure is too low and the time available before the product mixture is frozen in the expansion too short for this route to be important. In fact, when the partial pressures of initially produced NO_2 and dimethylamino radicals are increased by about a factor of ten, the consumption of NO_2 in secondary bimolecular reactions can be observed. Calibration of the detection system using known flows of laser-heated NO and NO_2 indicates the rearrangement/ N-NO_2 bond scission branching ratio (at about 900K) is ~ 0.7 . Thus, these results confirm the inferences drawn from the low temperature dependence consistently observed in the GC/MS-monitored nitramine pyrolysis. This work is described in detail in Appendix B, a manuscript to be submitted to the Journal of Physical Chemistry.

In ongoing studies under ARO support, we are probing the laser pyrolysis reactor still more directly, using laser-induced fluorescence (LIF) to determine the nascent NO/NO_2 ratio.

AB INITIO QUANTUM MECHANICAL CALCULATIONS

To further establish the significance of nitro-nitrite rearrangement as an initial step in decomposition of DMNA, for which we have obtained evidence in both of the laser-pyrolysis systems, we have undertaken a theoretical study of the rearrangement process in the analogous unsubstituted nitramine. Structures of NH_2NO_2 , the four isomers of NH_2ONO , dissociation products, and the transition state have been optimized using MCSCF analytic second derivatives with a 4-31G* basis set. The geometry of the transition state may be described as separated NH_2 and NO_2 fragments held together by dipole-dipole interaction. The N-N bond length is 2.85 Å, twice as long as at the NH_2NO_2 equilibrium geometry. The wave function of the transition state is characterized by two singly-occupied orbitals. Optimization of the transition state depends, therefore, on the use of MCSCF-based methods.

Energies have been obtained by large-scale multireference single- and double-excitation CI calculations with a 6-31G* basis set. The transition state is predicted to lie 46.68 kcal/m above NH_2NO_2 and 0.87 kcal/m below the $\text{NH}_2 + \text{NO}_2$ asymptote. Because the significant frequencies of the transition state are very similar to those of the separated fragments, the A factor for rearrangement should be not much less than that for bond scission. Assuming that results for the unsubstituted species may be applied directly to dimethyl-nitramine, the rates for nitro-nitrite rearrangement and N- NO_2 bond scission should be quite comparable in the latter system, in agreement with the results from the molecular-beam mass-spectrometrically monitored laser pyrolysis experiments reported above. However, we note that quantitative agreement with the temperature dependence observed in the GC/MS-monitored LPHP system would require an A-factor and activation energy substantially lower for the isomerization in order that the overall temperature dependence would be roughly midway between that for each of the competing initial steps.

Details of the theoretical study, which has been performed in collaboration with Dr. Megumu Yoshimine of IBM Almaden Research Center, are presented in Appendix C, a draft of a manuscript to be submitted to the Journal of Physical Chemistry.

NITRAMINE SYNTHESSES

In the course of repeated syntheses of dimethylnitramine, we developed a new route that is extremely convenient and safe for synthesizing dimethylnitramine and presumably other nitramines as well. This method involves nitration of the respective phosphoric triamide and avoids the nitrations that can be very hazardous, even at moderate scale. For dimethylnitramine, this method is extremely cheap and convenient, because it simply requires the commonly used solvent hexamethylphosphoramide. The synthesis of dimethylnitramine from hexamethylphosphoramide is described in the short manuscript included as Appendix D.

CONCLUSIONS

The result of the three approaches to understanding dimethylnitramine decomposition we have used in this research is a demonstration of the existence of a new initial reaction pathway for nitramines, a unimolecular nitro-nitrite rearrangement, followed by rapid scission of the extremely weak $(\text{Me})_2\text{NO}-\text{NO}$ bond. This pathway, which tends to be competitive with the expected $\text{N}-\text{NO}_2$ scission, is analogous to that shown recently for aliphatic- and aromatic-nitrocompounds, but had not been previously reported for nitramines. Recent dimethylnitramine decomposition results in the literature⁷⁻⁹ had in fact, been interpreted as evidence for exclusive $\text{N}-\text{NO}_2$ fission. The new nitro-nitrite rearrangement pathway may have relevance for the practical functioning of nitramines, since it leads directly to a more oxidized skeleton (and possibly to the various RDX nitrosamine products recently reported by Hofsommer and Glover in condensed phase decomposition¹⁶), but may well block the concerted (or sequential) depolymerization to the nitro-imine monomer units. The importance of the latter products is that they can lead directly to N_2O and formaldehyde, and thence, in a highly exothermic reaction, to N_2 , CO , and H_2O . Thus, changes in the branching ratios between nitro nitrite rearrangement and competing initial steps ($\text{N}-\text{NO}_2$ scissions and, in cyclic nitramines, depolymerization) may well help determine whether the decomposition process proceeds to a self sustaining stage. In more general terms, the results serve to emphasize the multiplicity of pathways available to nitramines, and the necessity, difficulties notwithstanding, for characterizing these pathways if the factors controlling nitramine ignition, initiation, and deflagration-to-detonation behavior are to be really understood.

REFERENCES

1. Shaw, P., Walker, F. E., J. Phys. Chem., 1977, 81, 2572.
2. Schroeder, M. A., "Critical Analysis of Nitramine Decomposition Results: Some Comments on Chemical Mechanisms," Proc. 16th JANNAF Comb. Mtg., CPIA, 14 September, 1979, Vol. 2, p. 17.
3. Fluornoy, J. M., J. Chem. Phys., 1962, 36, 1106.
4. Korsunskii, B. L., Dubovitskii, F. I., Sitonina, G. V., Doklady Akademii Nauk SSSR, 1967, 174(5), 1126.
5. Korsunskii, B. L., Dubovitskii, F. I., Doklady Akademii Nauk SSSR, 1964, 155(2), 402.
6. McMillen, D. F., Barker, J. R., Lewis, K. E., Trevor, P. L., Golden, D. M., "Mechanisms of Nitramine Decomposition: Very Low-Pressure Pyrolysis of HMX and Dimethylnitramine," Final Report, SRI Project PYU-5787, 18 June 1979 (SAN 0115/117). DOE Contract No. EY-76-C-03-0115.
7. Lloyd, S. A., Umstead, M. E., Lin, M. C., J. Energetic Materials, 1985, 3, 187.
8. Umstead, M. E., Lloyd, S. A., Lin, M. C., Proc. 22nd JANNAF Comb. Mtg., CPIA, 1985, p 512.
9. Wodtke, A. M., private communication.
10. Shaub, W. M., Bauer, S. H., Int. J. Chem. Kinet., 1975, 7, 509.
11. McMillen, D. F., Lewis, K. E., Smith, G. P., Golden, D. M., J. Phys. Chem., 1983, 86, 709.
12. Tsang, W., J. Chem. Phys., 1964, 40, 1498.
13. Gonzalez, A. C., Larson, C. W., McMillen, D. F., Golden, D. M., J. Phys. Chem., 1985, 89, 4809.
14. Tsang, W., Robaugh, D., Mallard, W. G., J. Phys. Chem., 1986, 90, 5968.
15. Batt, L., Robinson, G. N., "Thermochemistry of Nitro Compounds, Amines, and Nitroso Compounds," in Chemistry of Functional Groups: Supplement F, Ed., S. Patai, J. Wiley and Sons, Ltd., Chichester, 1981, p. 1035.
16. Hoffsommer, J. C., Glover, D. J., Comb. and Flame, 1985, 59, 303.

Appendix A

THERMAL DECOMPOSITION OF DIMETHYLNITRAMINE AND
DIMETHYLNITROSAMINE BY PULSED LASER PYROLYSIS

S. Esther Nigenda, Donald F. McMillen, and David M. Golden

(Submitted for publication in J. Phys. Chem., November 1987)

THERMAL DECOMPOSITION OF DIMETHYLNITRAMINE AND
DIMETHYLNITROSAMINE BY PULSED LASER PYROLYSIS

S. Esther Nigenda, Donald F. McMillen,
and David M. Golden
Department of Chemical Kinetics
SRI International, Menlo Park, CA 94025

ABSTRACT

Pyrolysis of dimethylnitramine (DMNA) and dimethylnitrosamine (DMNO) was carried out in a flow system over the temperature range 800 to 900 K using pulsed infrared laser heating, via SF₆ in a 250 torr bath of CO₂ and radical scavenger. Arrhenius parameters for DMNO and DMNA decomposition were $\log k(\text{s}^{-1}) = 15.8 \pm 1.1 - (50.0 \pm 3.4)/2.3RT$, and $13.5 \pm 0.6 - (37.4 \pm 2.5)/2.3RT$, respectively. The former set of parameters is consistent with simple bond scission as the rate limiting step; the latter set, which was produced with different scavengers, temperature standards, and varying amounts of added NO as a radical trap, is not consistent with simple bond scission. The experimental results can be reproduced via a mechanistic numerical model in which N-NO₂ bond scission and nitro-nitrite rearrangement are competitive initial steps and the displacement of NO₂ from DMNA by NO is included as a low temperature route to DMNO.

CK 87-47
Submitted to Kaufman Memorial Issue
J Phys Chem, 11/25/87

INTRODUCTION

Some years ago Fluornoy¹ reported that the decomposition of N,N-dimethylnitramine in static bulb experiments over the temperature range 165 to 200 K resulted in formation of N,N-dimethylnitrosamine in roughly 85% yield. He explained this product via recombination of NO and dimethylamino radicals. This reaction is in itself completely reasonable. However, Fluornoy found it necessary to invoke reactions that would produce NO in high yield, but these are somewhat vague and questionable, as discussed by Lin². Several years ago, we³ used the very low-pressure pyrolysis technique (VLPP) to examine dimethylnitramine decomposition at pressures in the millitorr range. More recently, Lin and co-workers have studied the decomposition of dimethylnitramine in both low temperature (466 to 524 K) static bulb experiments² and in single pulse shock tube work at much higher temperatures (800 to 1200 K).⁴ Lee and coworkers⁵ have also recently studied the infrared multiphoton decomposition of dimethylnitramine under collisionless conditions. The results of these and other workers are summarized in Table 1. In all but the two cases where the molecules are the most isolated (the multiphoton and the VLPP studies), the major product is dimethylnitrosamine. Thus, reaction leads to a product having the N-N bond intact, in spite of the fact that the initial reactions are presumed to have involved N-N bond scission of one sort or another. Reforming the N-N bond (e.g., through radical recombination with NO) is not in itself difficult, but for it and other secondary reactions to take place at rates such that dimethylnitrosamine is produced in almost quantitative yield is a result that one would not have predicted.

The general goal of this work is to determine the products of dimethylnitramine decomposition and the temperature dependence of the various rate-controlling processes, in order to help achieve the overall goal of understanding what controls the decomposition of cyclic nitramines and other energetic materials. Under almost all circumstances (all but low concentrations and/or very short time scales), the nature of these materials dictates that this means considering not only the initial steps but also a varying range of secondary reactions. This paper presents our results for the thermal decomposition of dimethylnitramine and dimethylnitrosamine using GC-MS monitored laser-powered homogeneous pyrolysis (LPHP). In this technique, the net decomposition in a flow system averaged over many laser pulses and over the entire volume of the cell is measured. A mechanistic numerical model accounting for the observed Arrhenius parameters, the products, and their relative yields is also presented. Complementary results obtained with a real-time molecular beam mass spectrometrically monitored version of LPHP are the subject of a paper to be submitted.

EXPERIMENTAL PROCEDURE

The pulsed laser pyrolysis technique used here (GC/MS-monitored) has been described in detail.⁸ Briefly, a CO₂ laser is used to heat the substrate (at 0.1 torr) via an absorbing but unreactive gas (e.g., SF₆ -10 torr), which then transfers its kinetic energy by collision (total pressure 100 torr, collision frequency = 10⁹/s), bringing the substrate to high temperature in 1-3 μs. For radical forming processes, scavengers and/or traps are necessary (e.g. toluene, cyclopentane, NO -5-20 torr) Reaction then occurs in the roughly 10 μs available before cooling takes place as the acoustic expansion wave moves radially inward toward the center of the cell. Figure 1 shows a schematic of the LPHP apparatus.

With the LPHP technique, surface catalyzed reactions at high temperatures are essentially precluded, since the time scale for heating, reaction, and cooling is far shorter than the millisecond time scale of diffusion to the walls. (Adsorption of IR-absorbing reactants or products on the KCl windows could conceivably result in decomposition of an adsorbed phase. This is generally unlikely, since only extremely strongly absorbing materials would be heated to a sufficiently high temperature when present at only a few monolayers thickness on the transparent, cold windows.)

The need to explicitly measure the temperature corresponding to any particular measurement of *k* is eliminated by use of the "comparative rate" technique.^{8,9} This involves concurrent determination of the fractional decomposition of a temperature standard, a second "substrate" (-0.2 torr) whose

decomposition rate temperature dependence is already well known, and therefore whose fractional decomposition defines an "effective" temperature that is a convolution of temperature over time and space within the heated portion of the cell. Given that the temperature dependence of the substrate and the temperature standard are not greatly different, and that the fractional decomposition of both materials is less than about 25%, the standard and the substrate "track" the temperature variations in a similar manner. Data reduction simply involves determining the slope and intercept of a plot of $\log k_{\text{unknown}}$ vs $\log k_{\text{standard}}$, which correspond to the ratio of activation energies and the difference in the $\log A$ values, respectively. As discussed in references 8 and 9, uncertainties in reaction time and in cell volumes cause no error in the derived activation energies (slope of the comparative rate plot) and only small errors in derived A-factors.

The extent to which the comparative rate method accommodates the temperature and reaction time variations inherent in this laser pyrolysis technique has been amply demonstrated by estimates of the errors involved and by testing the technique using a series of "unknowns" whose Arrhenius parameters have already been reported in the literature.^{8,9d} This has provided values in good agreement with the literature parameters for a series of molecular elimination reactions. The precision achievable indicates that the pulse-to-pulse and minute-to-minute laser variations that existed under the conditions of this experiment did not give rise to any distortion of the derived temperature dependence. Tests of this type make it clear that the comparative rate method, applied to pulsed laser pyrolysis, is very successful in accommodating the temperature variations inherent in the method and thereby providing an accurate measure of the temperature dependence of the substrate.

In this particular study, initial experimental difficulties included adsorption of substrates on the cell walls, premature decomposition of substrates and interference by chemical impurities. These difficulties were minimized and good mass balances obtained by silanizing the entire flow system including the gas reservoirs, carefully maintaining the lines and cell temperatures at 95°C (at lower temperatures, adsorption occurred; at higher temperatures, preliminary decomposition occurred), and by scrupulous purification of all compounds used. In particular, traces of NO₂ were removed from NO by passing it through 3 scrubbers containing 10 M NaOH, NaOH pellets, and molecular sieves, respectively. Special care was given to the elimination of NO₂ from NO, since the former readily gave rise to the nitrates and nitrites of the temperature standards used, thus distorting their decomposition temperature dependence.

RESULTS

A. Experiments

The thermal decomposition of dimethylnitramine was studied over the temperature range 780 K to 880 K. Figure 2 shows the decomposition rate of dimethylnitramine versus that of 4-hydroxy-4-methyl-2-pentanone (HMP) for two different experimental conditions. The rate expression¹⁰ for HMP is $\log k(\text{HMP} \rightarrow 2 \text{ acetone}) = 11.63 - 32.3/2.3RT$. In most cases an approximately 50- to 100-fold excess of radical scavenger, i.e. either toluene or cyclopentane, was used and the mass balance (decomposed material accounted for as product) for the temperature standard was 99±3%.

Excess nitric oxide was used in two of the runs shown in Figure 2 in order to trap any dimethylaminy radicals formed by the homolysis of the N-N bond in dimethylnitramine. Secondary reactions and products were thus minimized and dimethylnitrosamine accounted for 100±16% of the decomposed dimethylnitramine (for decompositions that were typically less than 10%). The least squares line drawn through the filled and un-filled squares is a composite of two runs performed under similar conditions. Toluene was used as the radical scavenger with a 50-fold excess of nitric oxide in one run (filled squares) and a 100-fold excess in the other (unfilled squares). As shown in Table 2, the Arrhenius parameters for the dimethylnitramine decomposition in the presence of excess NO, using either toluene or cyclopentane as the radical scavenger, are essentially the same, i.e., $\log k(\text{s}^{-1}) = 13.5 \pm 0.6 - (37.4 \pm 2.5)/2.3RT$.

Data obtained with toluene as the scavenger and in the absence of nitric oxide are also plotted in Figure 2. In this case no more than 60% of the decomposed dimethylnitramine could be accounted for, appearing as dimethylnitrosamine (25%), methylmethyleimine (~20%), nitrous acid (~12%), dimethylamine (~8%), and N,N-dimethylbenzylamine (~3). These yields varied with temperature, with the dimethylnitrosamine yield being smaller at the lower end of the temperature range. Trace amounts of N,N-dimethylacetamide were tentatively identified. Unlike runs with excess NO, in which virtually identical comparative rate plots are obtained either from reactant disappearance or product appearance, the comparative rate plot for data obtained in the absence of excess NO could only be based on the amount of dimethylnitramine lost. Nevertheless, as shown in the figure and in Table 2, the Arrhenius parameters obtained for dimethylnitramine decomposition in the absence of excess nitric oxide are still similar to those obtained in its presence.

Prior to using HMP as the temperature standard in the thermal decomposition of dimethylnitramine, t-butyl bromide was used as the temperature standard¹¹ in several runs in which the nature of the radical scavenger or of the nitrogen oxide present in the gas mixture was varied. The Arrhenius parameters obtained from the resulting comparative rate plots were similar to those obtained with HMP. However, due to experimental difficulties (see experimental section), attempted mass balances for both the temperature standard and the dimethylnitramine ranged widely. The quantitative results were therefore considered unreliable and are not reported here (even though the Arrhenius parameters generally fall within the range shown in Table 2). The following qualitative observations from these runs are nonetheless considered pertinent

in understanding this system's complexities and we attempted to incorporate them in the mechanistic modeling of the DMNA decomposition.

In the absence of excess nitrogen oxides, use of toluene as a radical scavenger resulted in the formation of N,N-dimethylbenzylamine, benzene and bibenzyl in addition to the formation of N,N-dimethylnitrosamine as the major product and formaldehyde in trace amounts. Use of cyclopentane as the radical scavenger gave, in addition to nitrosamine and formaldehyde, nitrocyclopentane and cyclopentene.

Since the reduction of NO_2 in secondary reactions is considered to be a critical step in dimethylnitrosamine production via recombination of the dimethylamino radical with NO , dimethylnitramine decomposition was also studied in the presence of toluene, t-butylbromide and roughly a 100-fold excess of nitrogen dioxide. Although a temperature standard was not included in this run, excess NO_2 appeared to have no substantial effect on the dimethylnitramine decomposition rate.

When the dimethylnitramine decomposition was carried out in the absence of radical scavenger or of nitrogen oxides, dimethylnitrosamine continued to be the major product, but formaldehyde was produced in more than 50% yield (relative to nitrosamine produced), and the rate of nitramine loss apparently increased by a factor of from 2 to 5. (The exact extent of acceleration is uncertain because the temperature standard was also absent in these runs.)

In order to check the behavior of our temperature standard, HMP, its Arrhenius parameters were independently determined using the LPHP comparative rate technique with t-butylbromide as the temperature standard (literature parameters¹¹ $\log k/s^{-1} = 13.8 - 41.8/2.3RT$). The A-factor and activation energy for HMP thus determined were in excellent agreement with those reported

in the literature¹⁰ ($\log A = 11.9$ vs 11.6 , and $E_a = 32.9$ vs 32.8 kcal/mol, respectively). This result, along with the good mass balances obtained for dimethylnitramine decomposition in the presence of excess nitric oxide and the similar Arrhenius parameters found for dimethylnitramine using *t*-butyl bromide as the temperature standard, all suggest that the Arrhenius parameters we report for dimethylnitramine are not distorted by systematic errors resulting from different temperature tracking behaviors.

Because of its importance as a product, the thermal decomposition of dimethylnitrosamine was also studied over the temperature range 870 to 990 K, using isopropyl bromide as the temperature standard. The comparative rate plot is shown in Figure 3. With dimethylnitrosamine the sequence of secondary gas phase reactions is considerably simpler than with dimethylnitramine since the formation of imine by loss of a hydrogen atom is, in the presence of scavenger, essentially irreversible, and the sequence of oxidation steps that take place when NO_2 is present cannot occur here. However, GC analysis of the imine presents a problem, since the proclivity of imines for polymerization reactions means that any surface contacted by the imine (e.g., in the heated transfer lines) is a candidate for promoting polymerization. The extent of this polymerization varies from day to day, exhibiting a sensitivity to factors not easily defined. Samples of the gummy polymer were collected and subjected to analysis by field ionization mass spectrometry (FIMS). The dominant peak in the pyrolysis/FIMS spectra of this material was m/z 86, corresponding to an imine dimer produced from thermal decomposition of the imine polymer.

The net result of this behavior is that, although the gas phase secondary reactions of dimethylnitrosamine are much simpler than for dimethylnitramine, reliable quantitative product analysis is very difficult. Hence the kinetics

were based solely on DMNO disappearance, and there is substantial scatter in the comparative rate plot. This scatter notwithstanding, the parameters extracted from the data in Figure 3 are consistent both with the expectation of simple N-NO bond scission as the rate-limiting step, and with the BAC-4 calculations of Melius¹² that suggest N-NO bonds are not weaker than their N-NO₂ counterparts, in marked contrast to C-NO bonds and their C-NO₂ counterparts.¹³ Thus, this result serves to reiterate that the LPHP technique behaves as claimed, and impels us to examine the chemistry more closely in the case of dimethylnitramine.

B. Numerical Modeling

In considering the data presented above, the goal was to choose a sequence of reactions that: (1) explained the observed products and the relative yield in which they are formed, (2) explained the observed overall rate parameters, and (3) did so with known or plausible parameters for each of the elementary processes. The mechanistic numerical model we constructed to help explain the results (decomposition of dimethylnitramine) consists of 75 primary and secondary reactions that account for all of the observed products. Reverse reactions were initially included for all reactions; some were dropped from the model when thermochemically limited parameters and numerical integration showed them to be of negligible importance. Certain reactions postulated in the literature as important contributors for the dimethylnitramine decomposition were retained in the model even if thermochemical limitations ruled out their importance.

The Arrhenius parameters for all reactions were taken from the literature where possible; otherwise they were derived by estimation techniques from analogous reactions in the literature. Where appropriate, the degree of falloff

was estimated by the RRK method. Instead of discussing each reaction and the parameters used for it individually, the main reactions in the model are schematically depicted in Figure 4. In Table 3 we list the rate parameters for the reactions included in Figure 4. We have endeavored to assure maximum utility for the modeling effort by remaining cognizant of the fact that literature data¹⁴ for all of the reaction types allow only a limited range within which the parameters can be varied without pressing the limits of plausibility.

In order to approximate the physical characteristics of the LPHP system and to account for the possibility of reaction during cooling (primarily low activation energy secondary reactions of radicals) of the laser-heated portion of the cell, the model incorporated a drop of 200K (from the initial 900K) at the end of the first time decade (10 μ s), followed by 100K drops at the end of each succeeding decade. The sequence of differential equations provided by the reactions was then integrated over time and temperature by a program that uses a numerical integration routine based on the Gear algorithm. The temperature profile and the computed dimethylnitramine concentration as a function of time is shown in Figure 5.

The experimental temperature dependence and product yields under different conditions were successfully reproduced only when the model included the nitro-nitrite rearrangement and also reactions 4, 6, and 11. These reactions are reversal of the nitro-nitrite rearrangement and of the nitrite thermolysis, and displacement of NO₂ from the nitrite by NO, respectively. The reasonableness of these reactions is considered in the following section; taken at face value, the computed values suggest that the experimental results do in fact reflect initial competition between simple bond scission and nitro-nitrite rearrangement, each with the parameters shown in Table 3.

DISCUSSION

As described in the preceding section, the mechanism whose important elements are shown in Figure 4 is able to reproduce the data, including nitramine decomposition rate parameters and dimethylnitrosamine yield under a range of experimental conditions, and furthermore does so with rate parameters for the various steps that are either experimentally determined or plausible extrapolations from related reactions. In this section, we examine the key steps in the model and discuss them relative to those that have been suggested in previous studies to account for observed rates and products.

The basic experimental results that must be duplicated if a dimethylnitramine decomposition mechanism is to be considered potentially valid are the decomposition rate and dimethylnitrosamine yield as a function of temperature and radical scavenger/trap concentrations. The difficulty that this seemingly simple requirement presents is that the experimental parameters are too low for simple bond scission to be the dominant rate-determining step, but any molecular elimination or rearrangement pathway that one writes to allow duplication of the Arrhenius parameters does not lead, by a simple sequence of known reactions, to the observed dimethylnitrosamine yields. Specifically, such sequences do not provide a route from the nitroxyl radical (which is the unavoidable scission product that follows nitro-nitrite rearrangement) to the nitrosamine.*

*One might have imagined that HONO from molecular elimination could take part in some surface-promoted nitrosation of amine during transport of the reaction products to the GC/MS system, but this would have involved reaction with the amine, rather than the imine. Furthermore, the imine tends to undergo a variable amount of polymerization on the walls of the the transfer lines; the observed yield of dimethylnitrosamine is quite reproducible, and therefore not easily connected with reactions subject to variations in surface conditions.

Given the notorious susceptibility of even precisely measured Arrhenius parameters to distortion by systematic error, we were initially inclined to assign the low temperature dependence to such distortions and conclude that the 100% yield of nitrosamine produced in the presence of excess NO simply resulted from trapping a quantitative yield of dimethylamino radicals produced in an initial N-NO₂ bond scission. However, rate measurements made under a wide range of experimental conditions that were employed in an effort to minimize distortion of the temperature dependence by spurious secondary reactions have repeatedly given $\log k(\text{s}^{-1}) = 13.5 \pm 0.5 - (37.4 \pm 1.5)/2.3RT$, as described in the preceding section. Furthermore, we conclude that there is no significant distortion of the temperature dependence by the highly reactive imine, since pyrolysis of dimethylnitrosamine, which yields the imine as the dominant product, produces a temperature dependence completely consistent with an N-NO bond scission. [Finally, preliminary results of dimethylnitramine pyrolysis in a molecular-beam mass spectrometrically sampled LPHP cell reveal that mass 60 and mass 30 (presumably dimethylnitroxyl radical and NO) are products of an initial unimolecular decomposition step.] Thus, the results indicating that a low A-factor initial step contributes to dimethylnitramine decomposition became too consistent to simply reject out of hand, and demanded a plausible mechanism that could account for them.

The critical reactions that make it possible for the numerical model to duplicate the low Arrhenius parameters and high dimethylnitrosamine yields in the presence of excess NO are shown in Figure 4 and Table 3, which have been abridged for purposes of discussion. The critical elements are:

1. N-NO₂ bond scission and NO₂-ONO rearrangement that are roughly competitive at 900 K (Reactions 1 and 3).

2. Rapid, but reversible thermolysis of the very weak O-NO bond in the N-nitrite (Reactions 5 and 6).
3. Reverse of the nitro-nitrite rearrangement (Reaction 4).
4. Attack of NO on the N-nitrite to displace NO₂ and yield directly the nitrosamine (Reaction 11).

The reverse of the nitro-nitrite rearrangement and of the nitrite thermolysis are required by microscopic reversibility (though we did not initially anticipate their impact). Reversal of the O-NO bond thermolysis is important only in the presence of excess NO, and it is only this reversal that can maintain a high enough steady state concentration of the weakly bonded nitrite such that reversal of the nitro nitrite rearrangement (Reaction 4) becomes significant. It is this latter reaction that allows some return to the nitramine and helps to limit the formation, under these conditions, of other products from the nitroxyl radical.

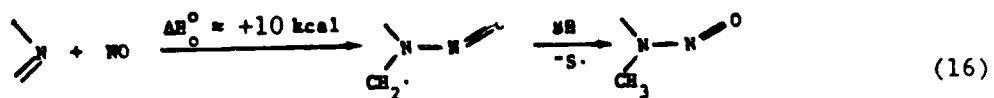
The only reaction in the sequence without direct precedent is reaction (11), the displacement of NO₂ from the nitrite by NO. This reaction is most important at lower temperatures. Because it is a low activation energy process and it limits return from the nitrite, it serves to substantially increase the net decomposition at low temperatures, while providing an additional route to nitrosamine. As an addition-elimination reaction between a free radical and a substrate having partial double bond character, it is the type of reaction that could well proceed with a low activation energy. As currently incorporated in the model, it has a 5 kcal/mol activation energy. If this is raised to 10 kcal/mol, the computed overall activation energy for DMNA loss is raised from 39.5 to 44.5 kcal/mol (i.e., 75% of the way to the 46.1 kcal/mol that results from complete elimination of reaction 11). There may conceivably be alternatives to reaction (11); as the reaction sequence is currently written, this reaction constitutes a necessary and reasonable route to nitrosamine from the

easily formed nitroxyl radical. That is, if nitrosamine is to be formed from the nitroxyl radical, the oxygen on the nitrogen clearly must depart, and departing as one of the oxygens on an NO_2 seems an eminently reasonable way to accomplish this. It is interesting to note that the stability of the nitroxyl radical at the same time makes it the inevitable product of the nitro-nitrite rearrangement and a bottleneck in the further decomposition of the amine framework. This bottleneck, in turn, is what evidently makes it possible for a major ultimate product of the nitro-nitrite rearrangement to be the nitrosamine.

In this and the following paragraphs, we consider some of the other reactions that have been previously suggested for nitrosamine formation. Beginning with the results of Fluornoy¹ some years ago, a number of suggestions have been made for the formation of dimethylnitrosamine as the main product from the thermal decomposition of dimethylnitramine. Two of these, namely unimolecular oxygen atom loss (15), and NO addition to the imine followed by scavenging of the resulting carbon-centered radical (16), can be ruled out on thermochemical grounds.

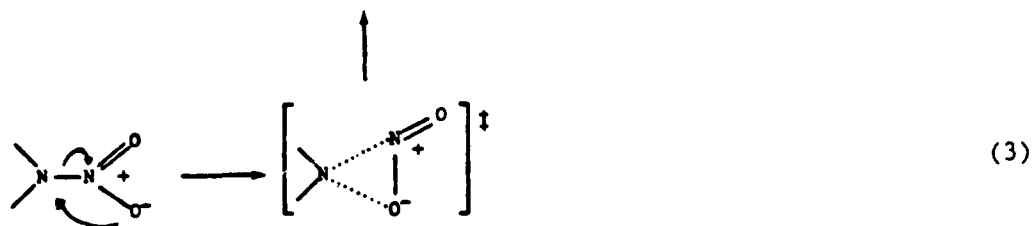
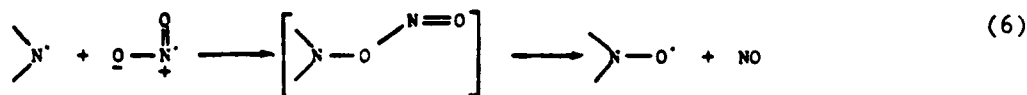
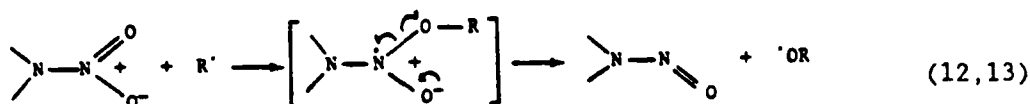


Reaction (15) is not a possible explanation because it has an endothermicity¹² substantially exceeding the observed activation energy for nitrosamine production.



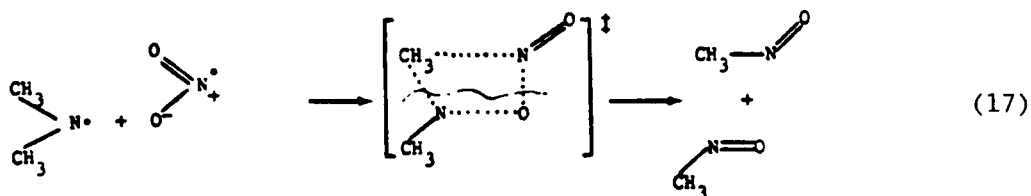
Reaction (16/16a) is unfavorable because the exothermic decomposition of the intermediate Reaction (-16) is much faster than its stabilization by any conceivable¹³ scavenger.

The remaining candidates that need to be considered include recombination of NO with the dimethylamino radical (9) as invoked by Lin,² radical addition to one of the nitro-group oxygens as discussed by Melius¹² (12,13) (i.e., direct bimolecular reduction of the intact nitramine), and bimolecular or unimolecular formation of the unstable O-nitroso compound (6,3) as an effective route to high yields of NO to serve as an intermediate for reaction (9).



The recombination of NO with the dimethylamino radical is the logical first candidate and has been invoked by all previous workers as a major source of nitrosamine; this step can be preceded by NO production routes consisting of a sequence of "known" unimolecular and bimolecular reactions (1 and 7) and/or by the nitro-nitrite rearrangement (3) which has precedent as a unimolecular process in nitromethane¹⁵ and nitrobenzene^{16,17} decomposition.

The four-center "recombination" leading directly to two nitrosomethane molecules suggested by Lin would appear to have steric requirements that are too stringent to be the high A-factor process that is evidently required to explain his observations.



On the other hand, Reaction (17) is not an unreasonable suggestion on enthalpic grounds, given the known tendency¹⁸ of C-nitroso compounds to dimerize.

The model used by Lin successfully reproduced his observed DMNA decomposition and DMNO formation rates through a route involving almost complete oxidative fragmentation of the amine structure and formation of NO as an intermediate in rather large yields in the process. However, there are several key steps whose parameters need to be carefully assessed in order to judge the adequacy of the reaction scheme as assembled by Lin. These are the four-center recombination (17) considered above, and the oxidation of the dimethylamino radical by NO₂ (7), and the thermolysis of nitrosomethane.

Reaction (17) can be viewed as a disproportionation with rather severe steric requirements. While the the impact of these requirements on the rate

may be tempered by the fact that the nitrosomethane dimer is bound¹⁸ by about 17 kcal/mol, an A-factor of $3 \times 10^9 \text{ l m}^{-1} \text{ s}^{-1}$ is still surprisingly high. Furthermore, for this reaction to take place to the exclusion of the recombination at an oxygen atom site (i.e., reaction 7), a known reaction that has no unusual steric requirements and leads to oxidation of the radical, is even more surprising. In principle, this "known" route can lead to the same products as the four-center recombination (17), since oxidation of the dimethyl amino radical gives a nitroxyl radical (7), which, upon β -scission, gives methyl radical and a molecule of nitrosomethane.



Thermolysis of nitrosomethane then gives NO and another methyl radical, which can go on to reduce more NO_2 to NO.



Whether the sequence of reactions (7), (18), and (19) will in practice give the same results as (17) and (19) is another question, since nitroxyl radicals are quite stable in general, and this particular one is estimated¹² to have a methyl-N bond strength of 44 kcal/mol.

Finally, the unimolecular dissociation (19) of the nitrosomethane itself is another step at which a bottleneck must be avoided, if the recombination route to nitrosomethane is to satisfactorily explain the various experimental results. The parameters that Lin² has evidently found necessary for this step to be fast enough include an A-factor of $5 \times 10^{16} \text{ l m}^{-1} \text{ s}^{-1}$. Values in the literature¹⁴ for loss of diatomic fragments, as well as consideration of the

overall entropy change in this particular reaction, indicate that 5×10^{16} is about an order of magnitude too large for nitrosomethane thermolysis, without consideration of the effects of falloff. In fact, use of all the other parameters chosen by Lin, but with the A-factor for this reaction lowered to 5×10^{15} , lowered the computed dimethylnitrosamine yield at 500 K from the observed 60% to 40%. These difficulties do not absolutely rule out NO recombination as the sole route to the nitrosamine, but serve at least to (a) quantify the intuition that a delicate balance among secondary reactions is required in order to produce enough NO for nitrosamine production through recombination, while still leaving enough intact dimethylamino radicals to recombine with the NO, and (b) amplify Lin's original finding that a fully satisfactory explanation does not easily follow from previously documented reactions.

A nitrosamine formation route that would not require a critical balance between amino radical survival and oxidative fragmentation is the one first made by Schroeder¹⁹ and recently subjected by Melius¹² to calculation by the BAC-MP4 method. If Reaction (12) is facile enough, it will result in rapid formation of the nitrosamine from virtually any radical produced in the system.

Reactions 12 (and 13) are quite reasonable: they are molecular analogs to the oxidation of radicals by NO_2 . Since they are not radical-radical reactions, but radical additions to a double bond, one might expect them to exhibit activation energies typical of those classes of reactions (1-2 kcal/mol for H-atoms, and 5-7 for carbon-centered radicals). However, the calculations of Melius¹² evidently suggest little or no activation energy for methyl radicals as well as for hydrogen atoms. Thus, in order to derive an upper limit to the possible importance of these reactions, we have incorporated them (for $\text{R} = \text{H}^\cdot$ and CH_3^\cdot) into the numerical model described above using

appropriate A-factors and zero activation energies for methyl radicals as well as hydrogen atoms. Under these conditions, the computation showed that reaction under the modeled temperature-time history illustrated in Figure 5 and in the presence of a 50-fold excess of toluene as radical scavenger resulted in a contribution to dimethylnitrosamine production from reactions 12 and 13 that was no more than 20% of the total yield of that product. Furthermore, the inclusion of these reactions did not lead to a tendency towards lower values. Thus, while they may be important during actual nitramine combustion, the nitrosamine formation reactions considered by Melius¹² would seem not to be responsible for the low A-factors and low activation energies observed under our scavenged laser pyrolysis conditions. In other words, we cannot, by inclusion of these reactions in the model, duplicate the observed temperature dependence for DNMA loss, namely an A-factor and activation energy two powers of ten and 10 kcal/mol, respectively, below those indicative of simple N-NO₂ bond scission.

SUMMARY

The decomposition temperature dependence and the product yields in the laser pyrolysis of dimethylnitramine can be accounted for by a combination of (1) competing unimolecular bond scission and nitro-nitrite rearrangement as the initial loss reactions, and (2) by a low temperature pathway to nitrosamine that involves reversals of the nitro-nitrite rearrangement and nitrite homolysis steps, coupled with a direct route from the unstable nitrite (or its oxidation state equivalent, the nitroxyl radical) to dimethylnitrosamine. Among these, the latter is the only reaction strictly without precedent; even it, as a displacement of NO_2 from the nitrite by NO is somewhat analogous to radical addition to a double bond. Parameters assigned to it on this basis allow the experimental observations to be reproduced without abandoning plausibility.

These results reveal competing initial reactions and facile secondary reactions in the decomposition of a simple nitramine. Understanding the range of possible reactions is clearly a necessary part of understanding the conditions required for the decomposition of this and more complex nitramines to become thermally self-sustaining. It is entirely fitting that our attempt to further this understanding is presented as part of a tribute to Fred Kaufman, who so aptly described endeavors such as this in his seminal plenary lecture²⁰ to the 19th Symposium (International) on Combustion. Experiments now underway with a different LPHP apparatus, in which the initial products of laser decomposition are detected directly via molecular beam mass spectrometry, will provide additional information about this competition.

ACKNOWLEDGEMENT

We acknowledge the support of the U.S. Army Research Office under contract No. DAAC03-86-K-0030, and the Air Force Office of Scientific Research under contract No. F49620-85-K-00006. We also thank Alicia C. Gonzalez for experimental efforts in the early part of this work.

DMG acknowledges the joy of having worked with and been a friend of Fred Kaufman. His enthusiasm, humor and essential humanity are sorely missed.

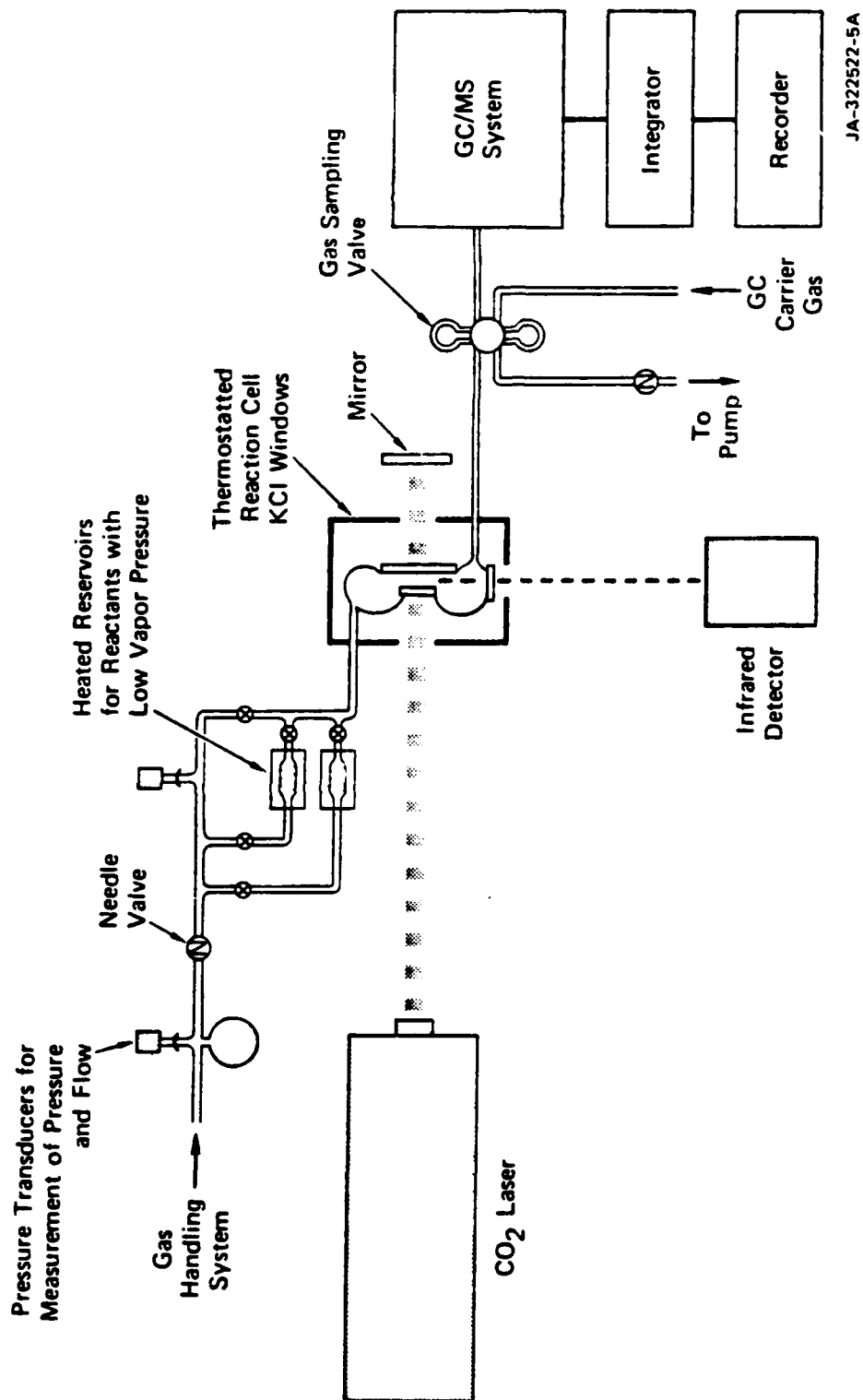
REFERENCES

1. Fluornoy, J. M. J. Chem. Phys., 1962, 36, 1106.
2. Lloyd, S. A., Umstead, M. E., and Lin, M. C., J. Energetic Materials, 1985, 3, 187.
3. McMillen, D. F., Barker, J. R., Lewis, K. E., Trevor, P. L., and Golden, D. M. "Mechanisms of Nitramine Decomposition: Very Low-Pressure Pyrolysis of HMX and Dimethylnitramine," Final Report, SRI Project PYU-5787, 18 June 1979 (SAN 0115/117). DOE Contract No. EY-76-C-03-0115.
4. Umstead, M. E., Lloyd, S. A., and Lin, M. C., Proc. 22nd JANNAF Comb. Mtg., CPIA, 1985, p 512.
5. Wodtke, A. M., private communication.
6. Korsunskii, B. L., Dubovitskii, F. I., and Sitonina, G. V. Doklady Akademii Nauk SSSR, 1967, 174(5), 1126.
7. Korsunskii and F. I. Dubovitskii, F. I., Doklady Akademii Nauk SSSR, 1964, 155(2), 402.
8. McMillen, D. F., Lewis, K. E., Smith, G. P., and Golden, D. M., J. Phys. Chem., 1983, 86, 709.
9. (a) Tsang, W. J. Phys. Chem., 1964, 40, 1171.
(b) Tsang, W., ibid., 1964, 41, 2487.
(c) Tsang, W., ibid., 1967, 46, 2817.
(d) Shaub, W. M., and Bauer, S. H., Int. J. Chem. Kinetics, 1975, 7, 509.
10. Smith, G. G. and Yates, B. L., J. Org. Chem., 1965, 30, 2067.
11. Tsang, W., J. Chem. Phys., 1964, 40, 1498.

12. Melius, C. F. and Binkley, J. S., "Thermochemistry of the Decomposition of Nitramines in the Gas Phase," Twenty first Symposium (International) on Combustion, The Combustion Institute 1987, 1988, p. 1953.
13. McMillen, D. F. and Golden, D. M., Ann. Rev. Phys. Chem., 1982, 33, 497.
14. see, for example, Kerr, J. A. and Moss, S. J., CRC Handbook of Bimolecular and Termolecular Gas Reactions, Vols. 1 and 2, CRC Press, Inc., Boca Raton, Florida, 1981; Tsang, W. and Hampson, "Chemical Kinetic Data Base for Methane Combustion," J. Phys. Chem. Ref. Data, 1986, 15, 1087-1279.
15. Wodtke, A. M., Hintska, E. J., and Lee, Y. T., J. Phys. Chem., 1986, 90, 3549.
16. Gonzalez, A. C., Larson, C. W., McMillen, D. F., and Golden, D. M., J. Phys. Chem., 1985, 89, 4809.
17. Tsang, W., Robaugh, D. and Mallard, W. G., J. Phys. Chem., 1986, 90, 5968.
18. Batt, L. and Robinson, G. N., "Thermochemistry of Nitro Compounds, Amines, and Nitroso Compounds," in Chemistry of Functional Groups: Supplement F, Ed., S. Patai, J. Wiley and Sons, Ltd., Chichester, 1981, p. 1035.
19. Schroeder, M. A., "Critical Analysis of Nitramine Decomposition Results: Some Comments on Chemical Mechanisms," Proc. 16th JANNAF Comb. Mtg., CPIA, 1978, 82, 644. 14 September, 1979, Vol. 2, p. 17.
20. Kaufman, F., "Chemical Kinetics and Combustion: Intricate Paths and Simple Steps," Nineteenth Symposium (International) on Combustion, The Combustion Institute, 1982, p. 1.

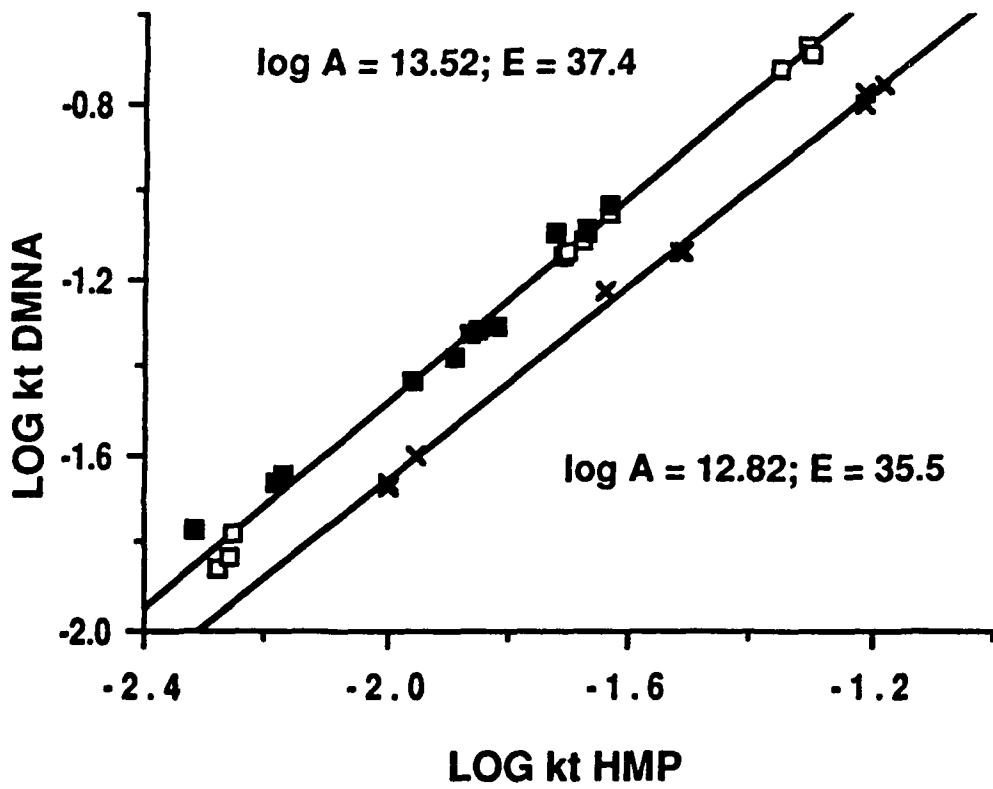
FIGURE CAPTIONS

- Figure 1 Schematic of GCMS monitored LPHP Apparatus.
- Figure 2 Comparative rate plot of dimethylnitramine (DMNA) vs 4-hydroxy-4-methyl-2-pentanone (HMP). ■ -50-fold excess of NO; □ -100-fold excess of NO; x-no additional NO; toluene as scavenger.
- Figure 3 Comparative rate plot of dimethylnitrasamine (DMNO) vs isopropyl bromide (iPrBr). (The different symbols represent experiments on different days.)
- Figure 4 Schematic representation of the mechanism at DMNA decomposition in the presence of excess NO.
- Figure 5 Schematic representation of the temperature changes with time imposed during numerical modeling to represent LPHP conditions. Also shown is the computed variation of DMNA with time. Initial conditions for model: cell temperature 367°C, $P_0(\text{DMNA}) = 0.11$ Torr, $P_0(\text{o-fluorotoluene})$, $P_0(\text{NO}) = 5.7$ Torr, $P_0(\text{hydroxy-methylpentanone}) = 0.11$ Torr.



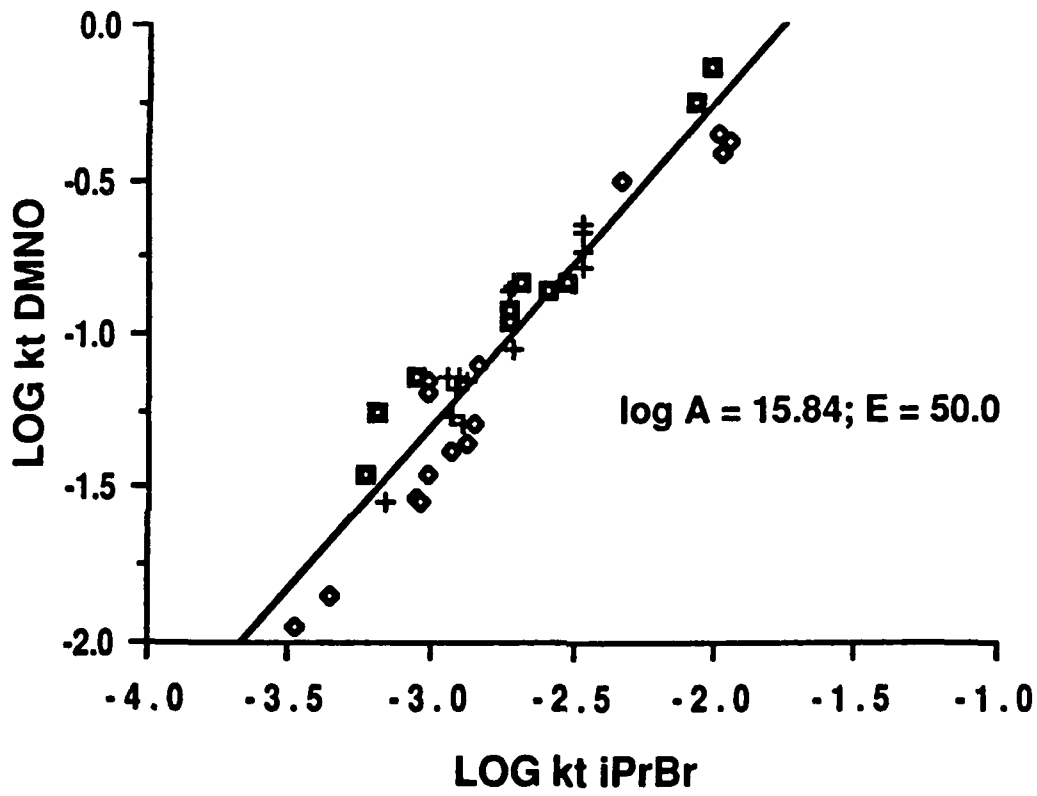
JA-322522-5A

Figure 1. Schematic of gas chromatographically monitored laser-powered homogeneous pyrolysis flow system.



JA-8232-1

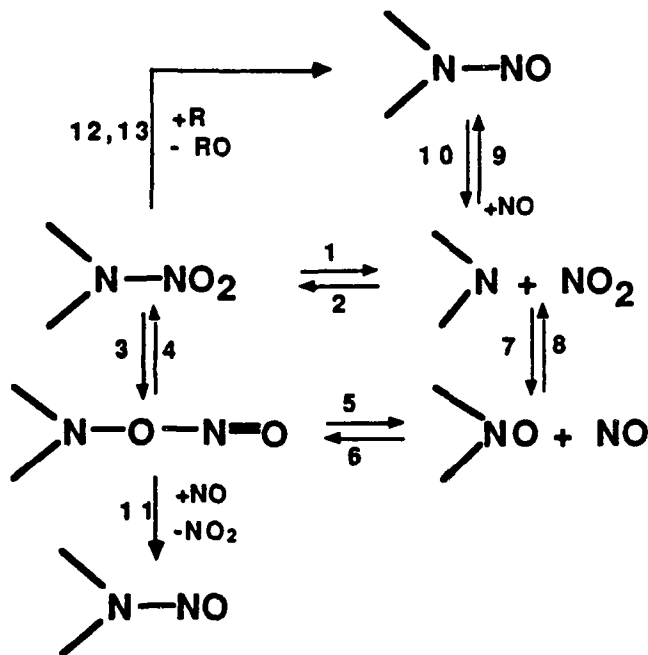
Figure 2



JA-8232-2

Figure 3

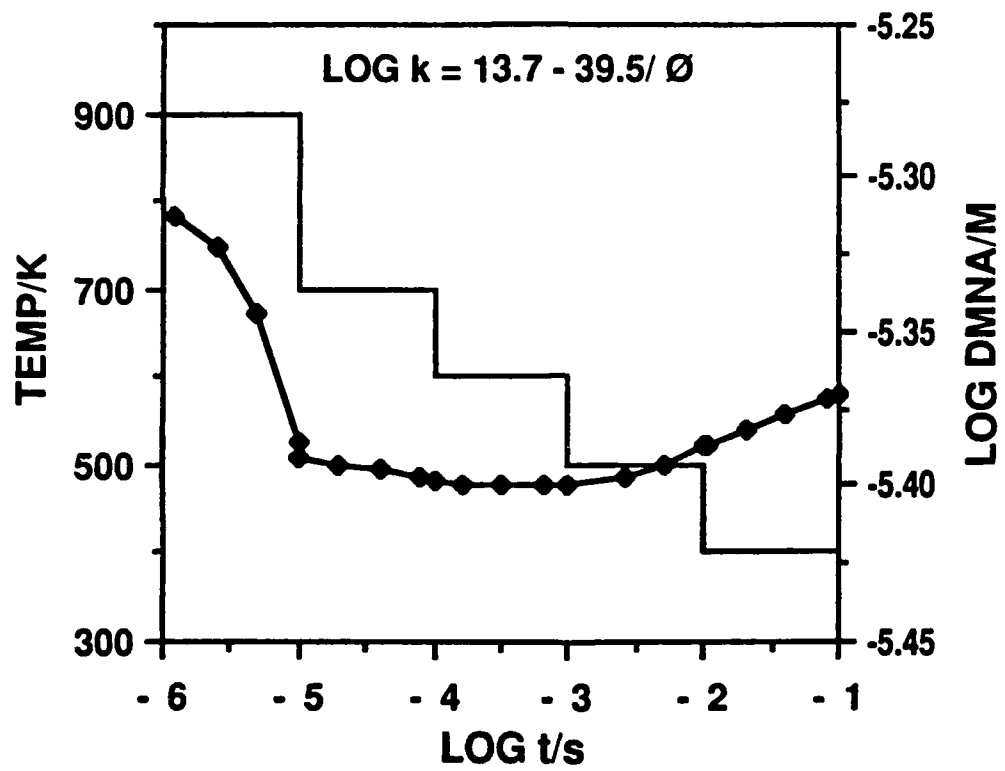
DMNA DECOMPOSITION MECHANISM



JA-8232-3

Figure 4

MODEL RESULTS



JA-8232-4

Figure 5

Table 1
Literature Parameters for Dimethylnitramine Decomposition

log A(s ⁻¹)	E(kcal/mol)	Technique	(T/K) Range	P/Torr	Reference/ Year
_____ ^a	_____	Molecular Beam MPD	_____	_____	Lee/1986 ⁵
15.9	44.1	Bulb/SPST	466-1000	474,3-6	Lin/1985 ⁴
16.5±0.5	45.4	Bulb	466-524	475	Lin/1985 ²
12.4	37.0	VLPP	560-850K	~10 ⁻³	McMillen/1979 ³
13.7	38.9	Bulb	450-510	~200	Korsunski/1987 ⁶
14.1	40.8	Bulb	450-530	64-400	Korsunski/1964 ⁷
20.1	53.0	Bulb	440-470	200-750	Flournoy/1961 ¹

^aProduct mass spectra and flight times consistent with N-NO₂ band scission.

Table 2
Laser Pyrolysis Comparative Rate Results for Dimethylnitramine

Temp. Std.	Scavenger	NO x Fold Excess	$\log[A/s^{-1}]$	$E_a/kcal/mol$	Nitrosamine Yield ^a
HMP	cyclopentane	100	13.5	37.4	113
HMP	toluene	100, 50	13.5	37.4	99
HMP	toluene	0	12.8	35.5	25

^a(Dimethylnitrosamine)/ Δ (Dimethylnitramine)

Table 3
Parameters Used in Numerical Modeling of Dimethylnitramine
and Dimethylnitrosamine Decomposition

No.	Reaction	log A ^a	E/kcal/mol
1	$(\text{CH}_3)_2\text{N} - \text{NO}_2 \rightarrow (\text{CH}_3)_2\text{N} + \text{NO}_2$	15.3	46.5
2	$(\text{CH}_3)_2\text{N} - \text{NO}_2 \leftarrow (\text{CH}_3)_2\text{N} + \text{NO}_2$	8.8	-2.0
3	$(\text{CH}_3)_2\text{N} - \text{NO}_2 \rightarrow (\text{CH}_3)_2\text{N-O-N=O}$	11.5	31.0
4	$(\text{CH}_3)_2\text{N} - \text{NO}_2 \leftarrow (\text{CH}_3)_2\text{N-O-N=O}$	10.5	11.1
5	$(\text{CH}_3)_2\text{N-O-N=O} \rightarrow (\text{CH}_3)_2\text{N-O}\cdot + \text{NO}$	13.7	9.0
6	$(\text{CH}_3)_2\text{N-O-N=O} \leftarrow (\text{CH}_3)_2\text{N-O}\cdot + \text{NO}$	9.9	0.0
7	$(\text{CH}_3)_2\text{N}\cdot + \text{NO}_2 \rightarrow (\text{CH}_3)_2\text{N-O}\cdot + \text{NO}$	10.0	0.0
8	$(\text{CH}_3)_2\text{N}\cdot + \text{NO}_2 \leftarrow (\text{CH}_3)_2\text{N-O}\cdot + \text{NO}$	9.9	13.8
9	$(\text{CH}_3)_2\text{N}\cdot + \text{NO} \rightarrow (\text{CH}_3)_2\text{N-NO}$	9.8	-2.0
10	$(\text{CH}_3)_2\text{N}\cdot + \text{NO} \leftarrow (\text{CH}_3)_2\text{N-NO}$	15.5	50.3
11	$(\text{CH}_3)_2\text{N-O-N=O} + \text{NO} \rightarrow (\text{CH}_3)_2\text{N-NO} + \text{NO}_2$	9.7	5.0
12	$(\text{CH}_3)_2\text{N-NO}_2 + \text{H}\cdot \rightarrow (\text{CH}_3)_2\text{N-NO} + \text{OH}\cdot$	10.0	0.0
13	$(\text{CH}_3)_2\text{N-NO}_2 + \text{CH}_3\cdot \rightarrow (\text{CH}_3)_2\text{N-NO} + \text{CH}_3\text{O}$	9.0	0.0

^aUnits of A are s^{-1} and $\ell(\text{m-s})^{-1}$ for unimolecular and bimolecular reactions, respectively.

Appendix B

MOLECULAR-BEAM-SAMPLED LASER PYROLYSIS OF DIMETHYLNITRAMINE

Paul H. Stewart, Jay B. Jeffries, Jean-Michel Zellweger,
Donald F. McMillen, and David M. Golden

(Submitted for publication in J. Phys. Chem., April 1988)

MOLECULAR-BEAM-SAMPLED LASER PYROLYSIS OF
DIMETHYLNITRAMINE

Paul H. Stewart,[†] Jay B. Jeffries, Jean-Michel Zellweger,[§]
David M. Golden and Donald F. McMillen
Department of Chemical Kinetics, Chemical Physics Laboratory
SRI International, Menlo Park, CA 94025

ABSTRACT

A pulsed CO₂ laser was used to heat a mixture of argon, SF₆, and dimethylnitramine (DMNA) in a flow cell, such that the periphery of the laser-heated region was immediately adjacent to a molecular-beam/quadrupole-mass-spectrometer sampling system. Detection of the product mixture in the molecular beam revealed that initial N-NO₂ scission was accompanied by a comparable amount of the nitro-nitrite rearrangement (followed by rapid scission of the extremely weak (CH₃)₂NO-NO bond) to produce directly NO and the nitroxyl radical. Production of this NO by secondary bimolecular reactions can be ruled out because the time available before the product mixture was frozen by expansion was too short, and because the observed rise times of the NO and NO₂ were identical. Calibration of the detection system with laser-heated NO and NO₂ at the reaction temperature (900 ± 50 °C) revealed that the rearrangement/bond-scission branching ratio is ~ 0.7:1.0. These results reveal that previous studies of dimethylnitramine concluding that N-NO₂ bond scission is the sole rate-limiting step are in error, and suggest that "loose" nitro-nitrite rearrangements may be a general phenomenon in N-nitro compounds as they appear to be in C-nitro compounds.

[†]Postdoctoral Research Associate.

[§]Present address: CIBA-GEIGY, CH-4333 Munchwillen/AG, Schweiz, Switzerland.

CK 88-25

Submitted to J. Phys. Chem., 4/88

INTRODUCTION

The initial decomposition step(s) of nitramines have been of interest for some time as one of the important keys to understanding what controls the initiation and combustion of nitramine explosives and propellants, respectively. For any energetic material this information tends to be difficult to obtain, since the utility of such materials is based on their tendency to undergo extremely rapid and exothermic decomposition once certain kinetic bottlenecks have been passed, thus obscuring the identity of the bottleneck reaction (or reactions). Furthermore, as has been appreciated for some time, the functionally useful nitramines have a multiplicity of candidate initial steps that can be identified on the basis of existing thermochemical information; however, this information is not sufficiently precise or reliable to allow an a priori distinction among the various candidates. Finally, the situation is further aggravated because secondary bimolecular reactions of radicals with NO_2 are known to be extremely fast and can be expected to complicate attempts to disentangle the reaction sequence.

For all of the above reasons, dimethylnitramine (DMNA) has been studied by various workers as a simple analog expected to exhibit some of the reactions that are important for the cyclic nitramines. However, the apparent simplicity of DMNA notwithstanding, it has been difficult to determine with certainty the initial decomposition step(s). Original work by Fluornoy¹ and by Korsunskii and coworkers² identified N- NO_2 bond scission as the initial step, although this was a matter of assignment rather than demonstration, as the temperature

dependence of the initial step was obscured to an uncertain degree by secondary reactions. More recently, Lin and coworkers³ reported low-temperature static bulb experiments and high-temperature single-pulse shock tube results, which when coupled together give an activation energy, measured over a wide temperature range that is indicative of initial N-NO₂ bond scission. Similarly, Wodtke and Lee⁴ have made preliminary reports of infrared multiphoton decomposition in a molecular beam also leading to the conclusion that N-NO₂ is the exclusive (i.e., ≥ 95%) initial reaction. In contrast with these results and concurrent with the work of Lee, comparative rate GC-analyzed laser pyrolysis experiments in this laboratory repeatedly gave a temperature dependence for DMNA decomposition that is not consistent with initial N-NO₂ bond scission.⁵

A choice between those results supporting and those contravening N-NO₂ bond scission as the sole rate-limiting step cannot be made without reservations. The shock-tube and static-bulb work¹⁻³ were performed without radical scavengers, and there is therefore no assurance that the decomposition rates are not perturbed by secondary reactions. In particular, for single-pulse shock-tube kinetic studies of hydrocarbon decomposition, there is a general need for scavengers to inhibit hydrogen atom chain reactions, when those are structurally possible. In the case of the multiphoton decomposition of DMNA in a molecular beam, there is, of course, no doubt that bimolecular secondary reactions are precluded. However, in the molecular beam of Wodtke and Lee,⁴ the sole diagnostic was the kinetic energy distribution of the m/z 30 signal, where the diagnosis that none of the mass 30 signal was actually NO coming from a molecular rearrangement depended upon the inability to detect, the presence of a component with a slightly shorter flight time (than m/z 46 and the m/z 30 signal that arises from ionization and ion fragmentation of NO₂).

The literature data outlined above, its limitations notwithstanding, together with our own previous experience with dimethylnitramine,⁵ led us to expect that N-NO₂ bond scission would be the dominant, and perhaps exclusive, reaction at 900 K. Thus, when we repeatedly obtained, in GC-monitored laser pyrolysis experiments,⁶ a temperature dependence indicative of a contribution from a low A-factor process, we responded by changing reaction conditions in search of a suspected systematic error. When these efforts, which involved varying the partial pressures and identities of the radical scavengers and the temperature standard, and the use of NO as a radical trap, all still resulted in a temperature dependence too low to indicate N-NO₂ as the sole rate-determining step, we concluded that direct observation of the initial step(s) was indicated. In this paper, we describe the molecular-beam-sampled, mass spectrometric detection of the initial products from the SF₆-sensitized laser pyrolysis of dimethylnitramine.

EXPERIMENTAL PROCEDURE

The thermal decomposition of dimethylnitramine was studied using a laser-powered homogeneous pyrolysis system coupled with a molecular-beam/mass spectrometer detection system. A pulsed CO_2 laser was used to irradiate a flowing mixture of sulphur hexafluoride (SF_6) absorber molecules, argon bath gas, and DMNA substrate. Following collisional energy transfer, the heated DMNA thermally decomposed. A molecular beam of the heated gas was formed by pumping it through a 75- μm diameter nozzle. The beam was then analysed using a quadrupole mass spectrometer (QMS), which allowed the direct detection of initial reaction products.

Flow System

The reaction mixture was prepared by establishing a flow of a commercially prepared 10% SF_6 /argon mixture (Matheson) through a glass tube containing the DMNA. The total pressure was maintained at a constant level (30 to 90 Torr) using a pressure regulator and controlling the pump-out rate of the cell. The "reservoir" tube containing the DMNA extended into the heated flow cell through an O-ring-sealed Cajon fitting (Figure 1). In this manner, controlled amounts of the nitramine vapor were introduced into the flow. The end of the glass reservoir was positioned as close to the laser-heated region as possible (to minimize surface effects). The aluminum reaction cell was maintained at a temperature typically in the range 25-35°C. The gas mixture was irradiated through the KCl windows at 2.0 Hz by a pulsed 10.6- μm CO_2 -laser beam of energy

$\leq 1.8 \text{ J/cm}^2$ and $1\text{-}\mu\text{s}$ duration. A mechanical pump was used to control the gas flow at a rate that insured complete renewal of the reaction mixture between laser pulses (0.5 s). The laser-heated region was cylindrical in shape, 1.1 cm in diameter and 2.5-cm long. The laser beam was positioned to irradiate the reaction mixture as close as possible ($\leq 1\text{mm}$) to the nozzle, so that the expansion wave generated by the laser heating pushed the gas inside the nozzle. Thus, a few microseconds after the laser pulse, the mixture was frozen by the adiabatic expansion, and radicals formed in the early process of decomposition were transported without undergoing further collision to the QMS in less than a millisecond.

Beam-Sampling System

The supersonic divergent nozzle consisted of a platinum disk (0.80 cm in diameter and $100 \mu\text{m}$ thick) with a $75\text{-}\mu\text{m}$ -diameter hole at its center (Ernest F. Fullam, Inc., Latham, NY). This disk was positioned at the apex of a conical support and held firmly in place by a screw-cap. A skimmer (electroformed nickel, Beam Dynamics, Minneapolis, MN) with a $200\text{-}\mu\text{m}$ diameter at the throat extracted the central portion of the beam. The distance between the nozzle and the skimmer entrance could be varied from a few millimeters up to 20 mm by external adjustment of a micrometer screw. A twin-bladed knife-edged chopper positioned at the entrance to Chamber 2 (containing the QMS) allowed the option of chopping the beam. The chopper operated at $\approx 650 \text{ Hz}$.

Molecular-Beam and Mass Spectrometer-Detection System

The molecular-beam laser-pyrolysis system was constructed from 304 stainless steel with three differentially pumped chambers, each evacuated with oil

diffusion pumps with freon-refrigerated baffles (Figure 2). The second chamber contained an Extranuclear Laboratories quadrupole mass spectrometer with electron impact ionization and ion-extraction perpendicular to the beam. The position of the QMS was adjustable from the outside by three screws and a bellows suspension. The bulk of the neutral beam passed through the differentially pumped ionizer region and impinged on a liquid-nitrogen cold trap. The cold trap prevented buildup of nitramine in the background gas during operation. The entire pumping system could be degassed by heating up to 200°C. The ultimate pressure (with no beam) was on the order of 10^{-7} torr in each chamber.

Data Acquisition

The mass-selected ions were accelerated into an electron multiplier. With the infrared heating laser off, the CW molecular beam could be chopped, and the signal for a specific ion mass could be phase-sensitively detected using a lock-in amplifier (ITHACO, Dynatrac 391). The QMS could then be accurately tuned into any particular mass by fine adjustment of the mass tuning to give the maximum signal on the lock-in amplifier. The QMS resolution was always better than 0.5 amu and was checked periodically.

With the QMS tuned into a specific mass and with the chopper off, the heating laser was pulsed. The infrared light passed through the cell, and absorption by the SF₆ heated the contents of the cell. Laser light was used to trigger a 1 MHz (sampling rate 1 μs per point) transient digitizer controlled by a DEC LSI 11/23 microprocessor to acquire the QMS signal. To improve signal-to-noise ratios, the signals from 2000-3000 laser shots were averaged. As a check that no product build-up was occurring during the experiment, the laser was switched off and the process repeated. In this case, a pulse

generator operating at 50 Hz was used to trigger the digitizer. The entire process was repeated for every mass studied. At the end of the experiment, the gain of the ion detector was measured by observing the variation of the CW molecular-beam signal with the high voltage. This "gain factor" was found to be mass independent and constant over long periods. The nitramine reservoir was then removed and the background levels in the vacuum chamber for all masses of interest were measured.

Data Reduction

Three operations were carried out on the raw data for each mass to yield the final results. These are briefly described below:

- (1) The backgrounds were subtracted from the raw data. This operation corrected for all signals not directly from the beam, i.e., background pressure in the ionization chamber.
- (2) The background-corrected data was then multiplied by an appropriate "gain factor" corresponding to the high voltage used when collecting the signals from that mass. The magnitude of this factor was determined by arbitrarily selecting one-voltage as having a gain factor of 1.0 and then calculating the factor for all other voltages. This procedure corrected for the signal-enhancement effect of raising the high voltage and allowed direct comparison of the data from different masses.
- (3) The cracking, or fragmentation, of the dimethyl nitramine from the electron impact ionization, rather than thermal decomposition, resulted in substantial increments to some of the lower m/z signals. The magnitude of this enhancement was determined in two ways.
 - (a) With the laser off (no thermal decomposition), ac signals (if any) for each mass were read from

the lock-in amplifier. These readings were multiplied by the appropriate gain factor (see above), and divided by the reading at m/z 90 for the DMNA molecular ion, to yield the cracking pattern.

- (b) The digitizer was "pre-triggered" to record a signal prior to the laser firing, such that the first millisecond or so of each temporal profile corresponded to unheated gas. Subtraction of the background resulted in a value for the signal analogous to the lock-in reading for each mass. Using this measure of the unheated gas at each ion mass a nitramine cracking pattern was also obtained.

Both procedures resulted in similar values for the cracking pattern, Table 1. The exception was for contributions to $m/z = 44$. No accurate background could be determined for this mass since in order to remove the nitramine reservoir the vacuum had to be broken briefly with subsequent contamination by atmospheric CO_2 . As a result, only method (a) could be used for mass 44. Improved cell design is planned to eliminate this problem.

With the contribution to each mass's signal from mass 90 cracking known, it was straightforward to subtract the appropriate fraction of the mass 90 signal from each temporal profile. A similar correction to the m/z 30 (NO^+) profile was required to take into account the cracking of NO_2 . Separate experiments using the present apparatus to produce laser-heated NO_2 , had given a m/z 30: m/z 46 ratio of 2.1:1. Thus, once steps 1-3 above had been performed for m/z 46 and 30 (NO_2 and NO , respectively), 2.1x the m/z 46 profile was subtracted from the m/z 30 profile. The extent to which masses other than 90 and 46 fragmented could not be determined quantitatively in the present study. Some contribution at m/z 30 is perhaps expected from the dimethylnitroxyl

Table 1
CRACKING PATTERNS FOR DMNA AND NO₂

m/z	Cracking (Digitizer)	Cracking (Lock-in Amplifier)
90	1	1
74	0.137	0.073
60	0.339	0.298
59	0.018	0.027
46	0.126	0.109
45	0.087	0.107
44	- -	0.565
43	2.89	2.02
42	3.36	2.38
30	0.557	0.36
NO ₂ (Laser Heated)		
46	1	
30	2.1	

radical and/or nitrosomethane, but essentially no contribution is expected from dimethylamino radical, dimethylamine, or N-methylmethylenimine. In other words, it is highly unlikely that any first- or second-generation products of N-NO₂ bond split, except NO₂ itself, will make any significant contribution to the m/z 30 signal.

When all of the above corrections had been performed, the resulting temporal profiles corresponded to changes caused solely by the laser-induced thermal decomposition of the dimethyl nitramine. (Note that we have assumed the cracking pattern for dimethylnitramine is independent of whether the beam is formed from laser-heated nitramine or from near room temperature nitramine. Since the sampling results in rotational and some vibrational cooling, some "leveling" is expected for the effect of temperature on the cracking pattern, which are anticipated to be minor in the first place. Furthermore, the m/z of most interest here (30, 45, 46, 59, and 60), are not large peaks in the DMNA spectrum, and the corrections to the signal representing NO, NO₂, and the dimethylnitroxyl radical are minor. In the particular case of NO₂, cracking to give m/z 30, where the correction to the signal that nominally represents NO is large, the cracking patterns were determined for laser-heated NO and NO₂.)

RESULTS

A typical set of temporal profiles are shown in Figures 3-5. Figure 3 is a temporal profile of the buffer gas, argon. One would expect the signal level before and after the laser pulse to remain unchanged. However, the rapid heating of the reaction mixture propagated a shock wave within the reaction zone. The effects of this shock wave are evident in Figure 3. (It was found necessary to machine an insert for the aluminum block cell to fill as much as possible of the volume unswept by the laser, in order to minimize the effects of the shock waves.

These efforts to minimize the cooling and reheating that results from expansion and from reflected shock waves were at least partially successful, and examination of the m/z 40 profile for argon in Figure 3 (and the other figures, as well) reveals that they can be divided into several different regions. The first of these regions is from zero time to ~ 1.2 ms. In Figure 3 this corresponds to unheated argon, as explained above. The sharp spike immediately following this region was caused by the electrical discharge as the laser fired. It acted as a marker for the arrival of the laser light at the reaction cell. The large fluctuations in signal level following the spike were due to shock waves, caused by the rapid heating of the gas, reverberating around the cell and resulting in rapid changes in pressure and temperature. When no SF_6 was present, i.e., when no heating occurred, this phenomenon did not occur. The signal returned to a steady level after 2.8 ms. The level during this quiescent period was almost exactly the same as the level prior to

the spike. At ~ 5.0 ms a second series of shock waves was observed. Again, this phenomenon did not occur when there was no heating. All the raw data obtained showed exactly the same shock effects at exactly the same times with the region between 2.8 ms and 5.0 ms being apparently shock free. From these observations, we concluded that the region from 2.8-5.0 ms represented the unperturbed post-shock signal level for each mass.

The upper trace in Figure 4 is a temporal profile for dimethyl nitramine ($m/z = 90$). The same general features as those for argon can clearly be seen. As explained above, the level prior to the electronic spike corresponds to unheated gas and the level from 2.8-5.0 ms corresponds to the level after heating. In this particular case, the nitramine underwent ~ 12.5% decomposition.

The temporal profile for $m/z = 46$, NO_2 , is shown in Figure 4. Once again, the same general features can be observed. The reduction in intensity of the spike and the different shock pattern between the spike and 2.8 ms are a direct result of the correction for parent cracking. The subtractions involved in the cracking corrections (see above) did not always result in exact cancellation of the spike and shock patterns. To obtain exact cancellation one would require that the magnitude of the spike and shock patterns for each m/z signal be proportional to the cracking pattern used in the subtraction.

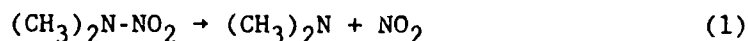
The shock patterns in Figure 4 were typical for all m/z signals, once corrected for cracking. It must be reiterated that the raw data for each mass show the same shock pattern as that for argon and dimethyl nitramine. The zero level in Figure 4 for $m/z = 46$, from $t = 0$ to the spike, is genuine; that is, following background, gain and cracking corrections, this level was indeed zero. This is as it should be, since there was no NO_2 present in the original reaction mixture. Had this level not been zero, it would have indicated a build-up

of reaction products between laser shots, i.e., the cell contents would not have been fully exchanged between shots. In fact, if the gas flow rate was decreased or the laser repetition rate increased, such a build-up was observed. A second check for product build-up was possible. Signal levels for each m/z were taken with the laser off (no heating) using a pulse generator as digitizer trigger (see above). Signal levels from $t=0$ to the spike, obtained with the laser firing, were compared with the laser-off values. If build-up were occurring, one would expect these two levels to differ. No such difference was observed. This was found to be the case for all other masses, i.e., the initial zero levels are all genuine.

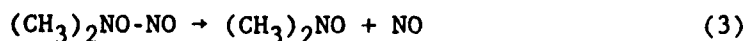
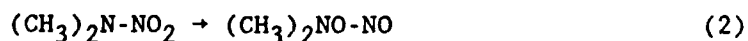
It is clear from Figure 4 that following the heating there is a sharp increase in the NO_2 level. In addition, the rate of increase of the NO_2 corresponds exactly with the decrease in the nitramine, indicating that the NO_2 was formed at the same time as the nitramine decomposed. This was also found to be the case for the signal change at all m/z , with one exception (see below). Figure 4 thus indicates that one thermal decomposition pathway for dimethyl nitramine gives nitrogen dioxide as an initial product.

Since the nitramine has a mass of 90 and NO_2 has a mass of 46, the expected counterpart to NO_2 at mass 46 in the DMNA decomposition is the dimethyl amino radical, mass 44. There is only a very slight increase in the m/z 44 signal, but quite clear increases in the levels of m/z 43 and 42, evidently the principal (and not unexpected) ion fragments of mass 44.

From the direct observation of these initial decomposition products it is clear that one decomposition pathway involves the cleavage of the N-N bond in dimethyl nitramine.



However, these were not the only initial products from the thermal decomposition of dimethyl nitramine. Masses 59, 45 and 30 were also produced (Figures 4-5). Each of these profiles exhibited the rise time indistinguishable from the rise of m/z 46 and the fall of DMNA at m/z 90. The elapsed time before the periphery of the laser-heated region expands into the nozzle is no more than $4 \mu\text{s}$; an upper limit to the fractional reaction of dimethylamino radical and NO_2 , based on extrapolated literature values⁶⁻⁸ for amino and methyl radical oxidation by NO_2 , can be placed at $\sim 5\%$. Thus, in order to explain the production of these species on a time scale appropriate only for a unimolecular reaction, one must invoke a nitro-nitrite rearrangement followed by O-N bond scission in the nitramine, reactions (2) and (3).



Reactions (2) and (3) explain the production of m/z 30, NO. Clearly, one would also expect to see the dimethylnitroxyl radical $(\text{CH}_3)_2\text{NO}$, mass 60. No significant change was observed in the $m/z = 60$ signal. However, the signals at m/z 59 and 45, which would correspond to loss of a hydrogen or a methyl group from the ionized nitroxyl species, are seen to increase substantially (Figure 5). This fragmentation almost certainly takes place in the ionizer and, given almost no change in the mass 60 signal, is evidently very facile.

From the direct observation of these initial reaction products it is clear that a second pathway for the thermal decomposition of dimethyl nitramine exists involving nitro-nitrite rearrangement followed by O-N bond scission. Calibrations using laser-heated NO and NO₂ performed under the same conditions as the dimethylnitramine decomposition, indicate that the ratio of rearrangement to simple bond-bond scission (k_2/k_3) is about 0.7.

In addition, the apparent mass balance for NO and NO₂ production and DMNA loss ranged from 1.05 to 1.33. This was based on the NO/NO₂ calibrations and the partial pressure of DMNA measured for the same set of flow conditions. Considering the assumptions made in determining this balance, this is good agreement and suggests that the various spectral subtractions, etc., have not introduced any substantial errors.

Only one other mass showed any discernable change after heating. This was $m/z = 74$, corresponding to the formation of dimethylnitrosamine, $(CH_3)_2N-NO$. Figure 6 shows temporal profiles for m/z 90, 46 and 74 obtained under conditions where secondary product buildup was occurring. In this case, a very small increase in m/z 74 occurred following the laser heating. However, the rise time was much longer than that for the other masses, supporting the expectation that the formation of dimethylnitrosamine was a result of secondary reactions, presumably the combination of $(CH_3)_2N$ and NO radicals.

DISCUSSION

The results presented above indicate that, in addition to N-NO₂ bond scission, a substantial fraction of dimethylnitramine (DMNA) decomposes, at temperatures of about 900 K, by way of an intramolecular rearrangement to the N-nitrite, followed by rapid scission of the extremely weak NO-NO bond. The interpretation is straightforward if the results presented above are taken at face value. The certainty attached to these results rests primarily with three factors. The first of these is the extent to which signal changes indicative of chemical reaction can be separated from the effects of reflected shock waves and gas-density fluctuations. The second is the extent to which spectral subtraction for m/z 30, 45, 59, and 60 correctly isolates the portions of these signals due to NO and dimethyl nitroxyl radical. The third factor is the certainty with which the observed rise time of the 30, 45, and 59 signals can be stated to be too fast to be accounted for by secondary bimolecular oxidation of dimethylamino radical by NO₂. The approach taken to deal appropriately with each of these factors is described in the results section; these approaches are elaborated below.

In considering factor number (1), fluctuations in intensity that are due to reflected shock waves and occur after the arrival of the first laser-heated materials, it should be reiterated that while there are short term (~ 250 μs) periodic fluctuations in the m/z 40 signal for the argon carrier due to density changes, there is no change in the signal averaged on a millisecond time scale. Therefore, changes on the latter time scale for reactive components actually

reflect chemical changes rather than mere gas-density fluctuations. As stated in the results section, we have chosen as the observation window the interval when the gas density changes reflected in the m/z 40 signal are minimal (3.2 to 4.5 ms). However, it is important to note that the results are not substantially dependent on this choice of a time window.

Examination of Figure 4, where the m/z 90, 46 and 30 intensities are plotted together, makes it clear that there are three steps of decreasing m/z 46 and 30 intensity (2.3 to 3.0, 3.6 to 5.2 and 5.8 to 6.8 ms) and that these are mirrored by three steps of increasing intensity in the m/z 90 profile. Thus, decreasing amounts of product NO_2 correspond to increasing amounts of the starting nitramine. The nozzle is evidently sampling in these three time periods, regions of successively lower values of $k_f dt$. While we have chosen, for the reason given above, to use the region from ~ 3.2 to 4.5 ms following the laser pulse, basically the same result is obtained if the region just prior to, or just after, it is used. In these latter regions, there will be somewhat more or somewhat less nitramine decomposition, respectively, and proportionately more or less product appearance from that decomposition. Thus, while the fractional decomposition is dependent on the chosen observation region, the distribution of product masses is not, making it very clear that the changes observed as one samples deeper and deeper into the laser-heated region, are not the result of (varying extents of) secondary reaction, but are the result of variations in temperature and reaction time.

The second factor bearing heavily on our principal conclusion is the extent to which ion fragmentation of species other than NO_2 and dimethylnitramine (which is quantitatively accounted for in the spectral subtraction) contributes to intensity at m/z 30, and thus might be responsible for apparent rapid

production of NO. Dimethylamino radical is not a likely source of m/z 30, since dimethylamine itself has almost no (< 2%) intensity at 30. It is, of course, likely that some of the m/z 30 arises from fragmentation of the molecular ion of the dimethylnitroxyl radical $(\text{CH}_3)_2\text{NO}$, but this in no way invalidates the main conclusion since the nitroxyl radical is the partner of intramolecularly produced NO. In fact, it is not unexpected that ion fragmentation of nitroxyl radical (m/z 60) might lead via CH_3NO to a substantial fragment at m/z 30. Accordingly, the intensities in Table 2 reflect use of the mass spectrum of nitrosomethane itself to make a rough estimate of the contribution of the nitroxyl radical to m/z 30. Given that there are no other obvious sources of mass 30, we are left with no alternative but to assign the m/z 30 intensity, once corrected for NO_2 , $(\text{CH}_3)_2\text{NNO}_2$, and CH_3NO cracking, to unimolecular production of NO.

Finally, confident assignment of the m/z 30 intensity in Figure 4 to intramolecular production of NO depends on the ability to preclude bimolecular reaction of initially formed dimethylamino radical and NO_2 as the source of the nitroxyl radical and NO. As stated in the results section, the time available for secondary bimolecular reaction is limited to the time before the laser-heated region expands the short distance (< 0.1 cm) to the sampling orifice. With this expansion taking place at roughly 1/3 sonic velocity, the available reaction time is less than 3 μs ; using $7 \times 10^9 \text{ l m}^{-1} \text{ s}^{-1}$ as an upper limit for NO_2 oxidation of dimethylamino radical (based on measured rates and temperature dependence for NO_2 reaction with methyl, amino, and acetyl radicals⁶⁻⁹, and the relevant entropy considerations⁹), one reaches the conclusion that no more than 5% of initially produced NO_2 could have been converted to NO by bimolecular reaction. Furthermore, as time passes, the expansion proceeds further and the

Table 2

CHANGE IN ION CURRENT ($t = 0$ to $t = 3.5$ ms) FOLLOWING LASER HEATING

m/z	Δ Ion Current	
90	5500 ^a	
60	~ 0	
59	260	
46 [*]	4260	2.9×10^{-9} mol cm ⁻³ ^b
45	660	
44	~ 0	
43	7421	
42	21310	
30 [†]	14100	2.2×10^{-9} mol cm ⁻³ ^b

^aCorresponds to ~ 12.5% depletion.

^bConcentrations determined from calibration experiments using Ar/SF₆/NO₂ and Ar/SF₆/NO mixtures.

^{*}Corrected for mass 90 cracking.

[†]Corrected for mass 90 and mass 46 cracking.

sampling takes place deeper into the laser-heated region. Thus, if secondary reactions were responsible for the observed NO, then the proportion of NO should increase with increasing time. As described in the results section,

such an increase is definitely not observed under the conditions of Figures 3 through 5. However, if the DMNA reservoir temperature is raised 30°C and the laser heating is increased so that the bulk of the DMNA is decomposed, then the partial pressures of initially produced NO₂ and dimethylamino radicals increase by an order of magnitude each, and the rate of bimolecular production of NO increases by two orders of magnitude. Under these conditions, we are able to see the NO₂ signal decrease, the NO signal grow substantially during the observation time and also to see a growth in m/z 74 (Figure 6).

CONCLUSIONS

The observation of substantial amounts of NO, together with the ion fragments of the dimethylnitroxyl radical, on the same time scale as NO₂ is produced, and much too rapidly for significant secondary bimolecular reaction, necessitates the conclusion that this rapidly produced NO arises from an intramolecular nitro-nitrite rearrangement, followed by extremely rapid unimolecular scission of the very weak O-NO bond. Although this is analogous to similar rearrangements that have been reported for nitroalkanes¹⁰ and nitroaromatics,^{11,12} it is in contrast with previous reports that dimethylnitramine decomposition proceeds entirely by N-NO₂ bond scission.¹⁻⁴ At this point, we presume that this reaction proceeds, as those in the C-NO₂ cases appear to, as a very "loose" rearrangement with rotation of the NO₂ not being substantial until there is considerable lengthening of the N-NO₂ bond. The nature of this rearrangement is now being explored in this laboratory (for unsubstituted nitramine) using multiconfiguration ab initio calculations.

Acknowledgement: We acknowledge the support of the U.S. Army Research Office under Contract No. DAAC03-86-K-003, and the U.S. Air Force Office of Scientific Research under Contract No. F496220-85-K-00006. The Chemical Physics Laboratory computer system (VAX 11/750) was purchased under NSF Grant No. PHY-8114611.

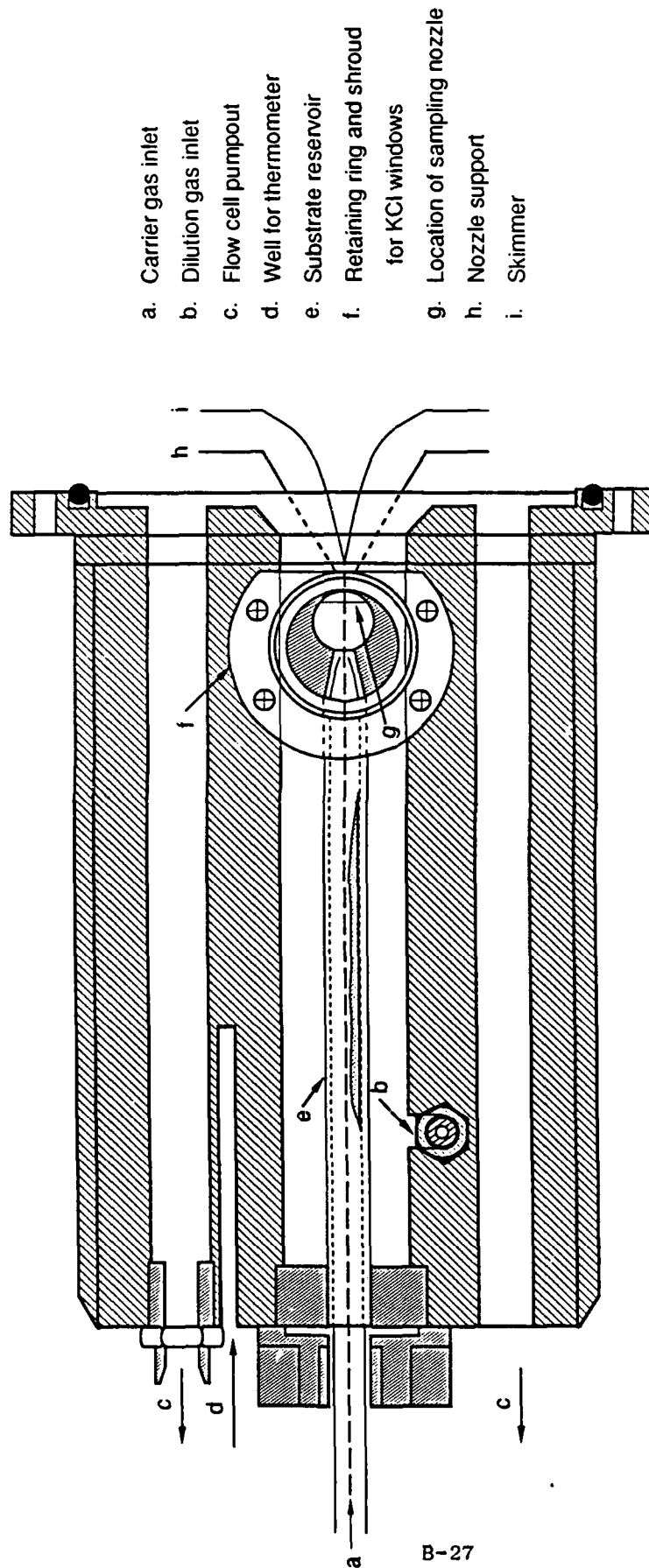
REFERENCES

1. Fluornoy, J. M., J. Chem. Phys., 1962, 36, 1106.
2. (a) Korsunskii, B. L.; Dubovitskii, F. I.; Sitonian, G. V.,
Doklady Akademii Nauk SSSR, 1967, 174(5), 1126.
(b) Korsunskii, B. L.; Dubovitskii, F. I., Doklady Akademii Nauk SSSR, 1964, 155(2), 402.
(a) Lloyd, S. A.; Umstead, M. E.; Lin M. C., J. Energetic Materials, 1985, 3, 187.
(b) Umstead, M. E.; Lloyd, S. A.; Lin, M. C., Proc. 22nd JANNAF Combustion Mtg., CPIA, 1985, p.512.
4. Wodtke, A. M., private communication.
5. McMillen, D. F.; Barker, J. R.; Lewis, K. E.; Trevor, P. L.; Golden, D. M., "Mechanisms of Nitramine Decomposition: Very Low-Pressure Pyrolysis of HMX and Dimethylnitramine," Final Report, SRI Project PYU-5787, 18 June 1979 (SAN 0115/117). DOE Contract No. EY-76-C-03-0115.
6. Nigenda, S. E.; McMillen, D. F.; Golden, D. M., submitted to J. Phys. Chem.
7. Yamada, F.; Slagle, I. R.; Gutman, D., Chem. Phys. Lett. 1981, 83, 409.
8. Slagle, I. R.; Gutman, D., J. Am. Chem. Soc., 1982, 104, 4741.

9. DeMore, W. B.; Margitan, J. J.; Molina, M. J., Watson, R. T.; Golden, D. M.; Hampson, R. F.; Kurylo, M. J.; Howard, C. J.; Ravishankara, A. R., "Chemical Kinetics and Photochemical Data for Use in Stratospheric Modeling," National Aeronautics and Space Administration, JPL Publication 85-37.
10. Benson, S. W., Thermochemical Kinetics, 2nd Ed.; Wiley: New York, 1976.
11. Wodtke, A. M.; Hintsa, E. J.; Lee, Y. T., J. Phys. Chem., 1986, 90, 3549.
12. Gonzalez, A. C.; Larson, C. W.; McMillen, D. F.; Golden, D. M., J. Phys. Chem., 1985, 89, 4809.
13. Tsang, W.; Robaugh, D.; Mallar, W. G., J. Phys. Chem., 1986, 90, 5968.

CAPTIONS

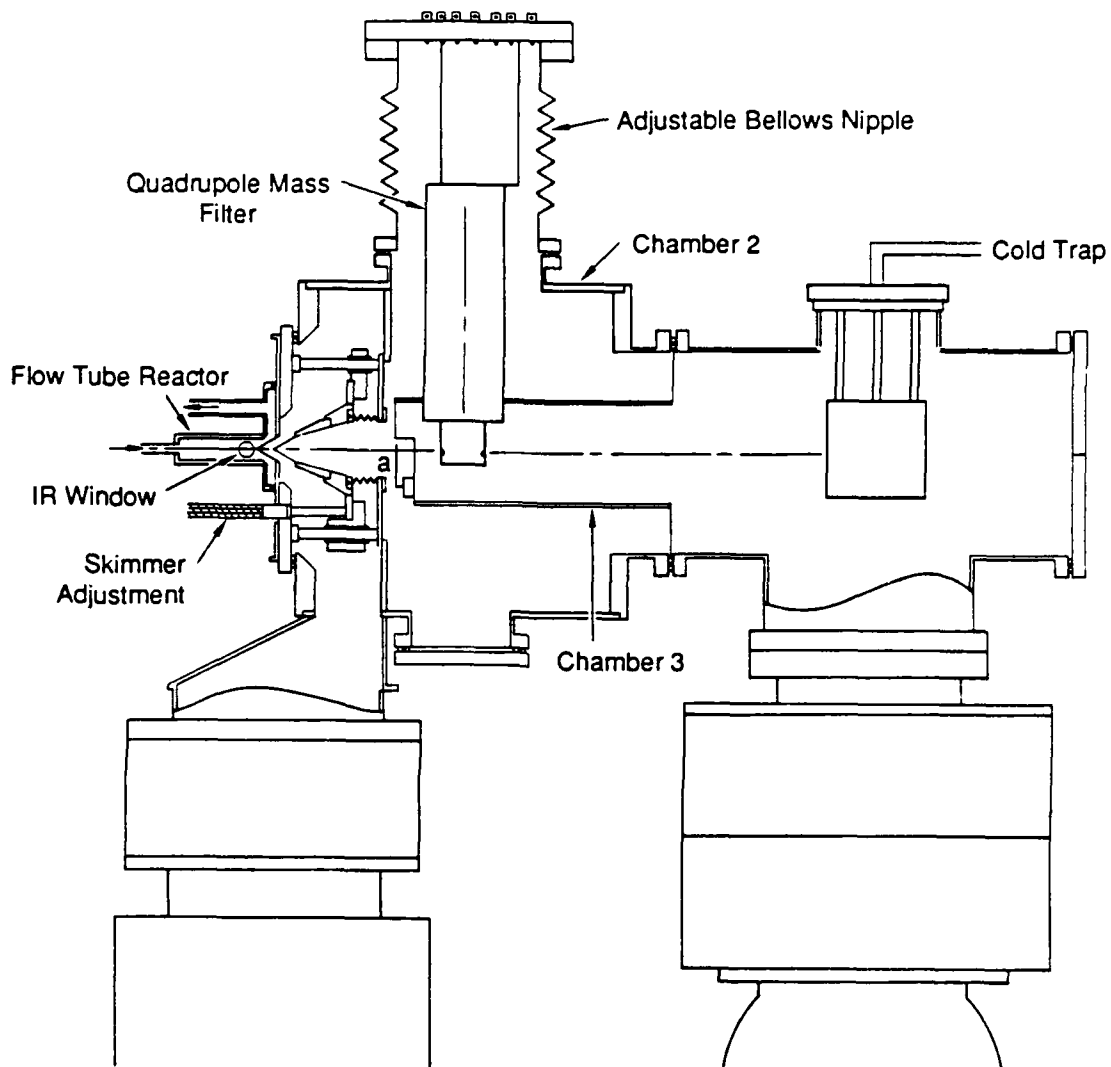
- Figure 1 SCHEMATIC DRAWING OF THE MACHINED ALUMINIUM FLOW CELL.
(a) carrier gas inlet; (b) dilution gas inlet; (c) flow cell pumpout; (d) well for thermocouple; (e) substrate reservoir; (f) retaining ring and shroud for KCl windows; (g) location of nozzle; (h) nozzle support; (i) skimmer.
- Figure 2 SCHEMATIC DRAWING OF THE MOLECULAR-BEAM-SAMPLED, MASS SPECTROMETRICALLY DETECTED LPHP SYSTEM.
For the sake of clarity, the diffusion pump associated with Chamber 2 has been omitted; (a) chopper.
- Figure 3 TEMPORAL PROFILE FOR m/z 40.
(a) electronic spike; (b) signal fluctuations induced by reflected shock waves; (c) quiescent period.
- Figure 4 TEMPORAL PROFILES FOR m/z 90, 46, and 30.
Changes in m/z 90 are mirrored by m/z 46 and 30. The rise times for m/z 46 and 30 are identical and correspond exactly to the drop in m/z 90 signal.
- Figure 5 TEMPORAL PROFILES FOR m/z 45 and 59.
Both profiles exhibit the same rise time as m/z 46 and 30.
- Figure 6 TEMPORAL PROFILES FOR m/z 90, 46, and 74.
Obtained under different conditions than those in Figures 3-5. The rise time for m/z 46 corresponds to the fall in m/z 90. However, the rise time for m/z 74 is much slower than for m/z 46 indicating that this species was formed by secondary reactions.



- a. Carrier gas inlet
- b. Dilution gas inlet
- c. Flow cell pumpout
- d. Well for thermometer
- e. Substrate reservoir
- f. Retaining ring and shroud for KCl windows
- g. Location of sampling nozzle
- h. Nozzle support
- i. Skimmer

JA-M-8232-6

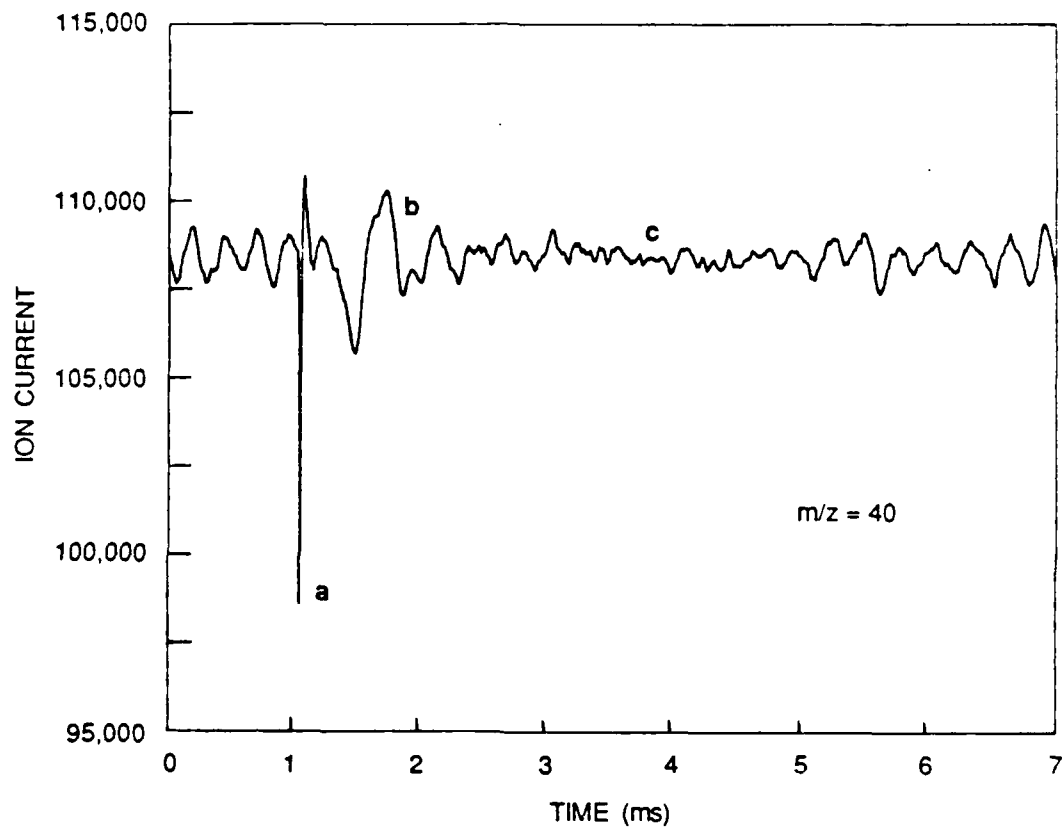
Figure 1. Schematic drawing of the machined aluminum flow cell.



JA-4814-1B

Figure 2. Schematic drawing of the molecular-beam-sampled, mass spectrometrically detected LPHP system.

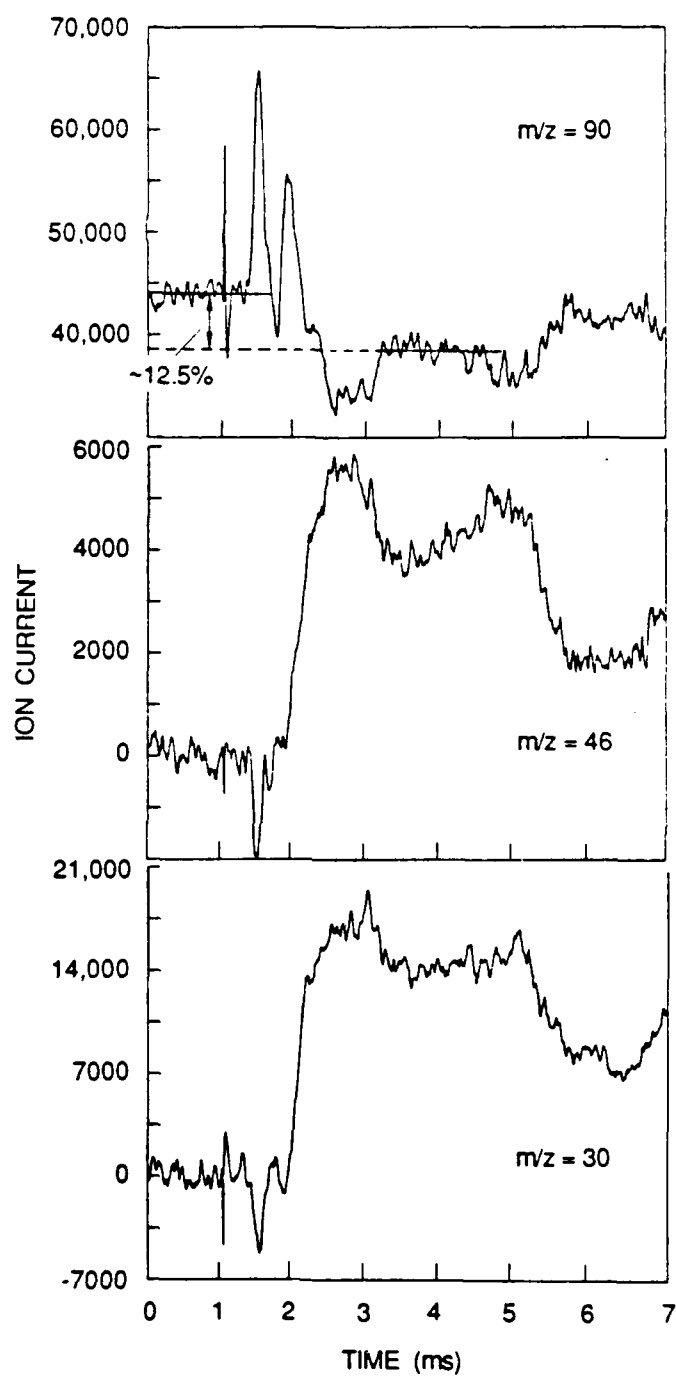
For the sake of clarity, the diffusion pump associated with Chamber 2 has been omitted; (a) chopper.



JA-8232-7

Figure 3. Temporal profile for m/z 40.

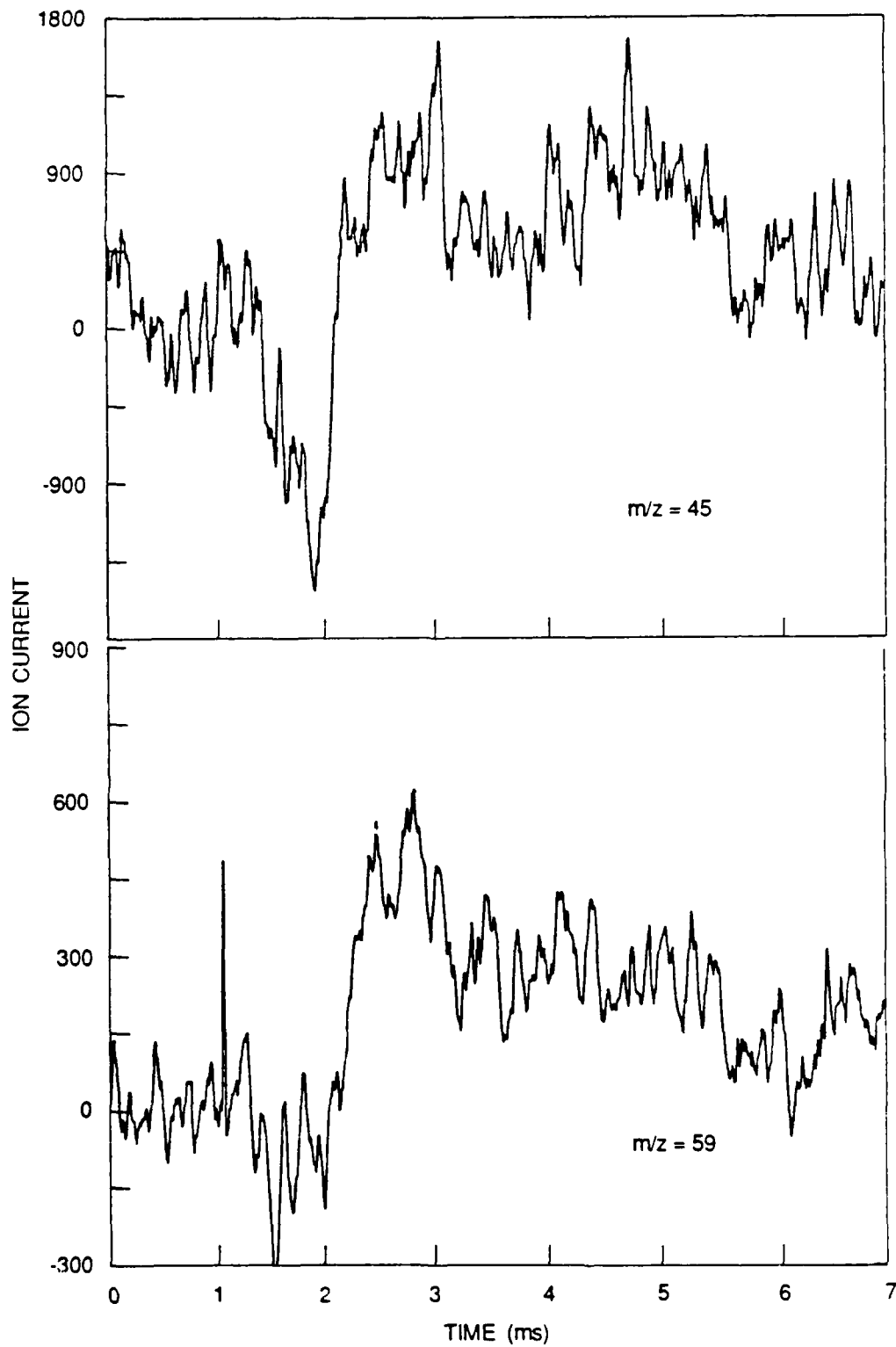
(a) electronic spike; (b) signal fluctuations induced by reflected shock waves; (c) quiescent period.



JA-8232-8

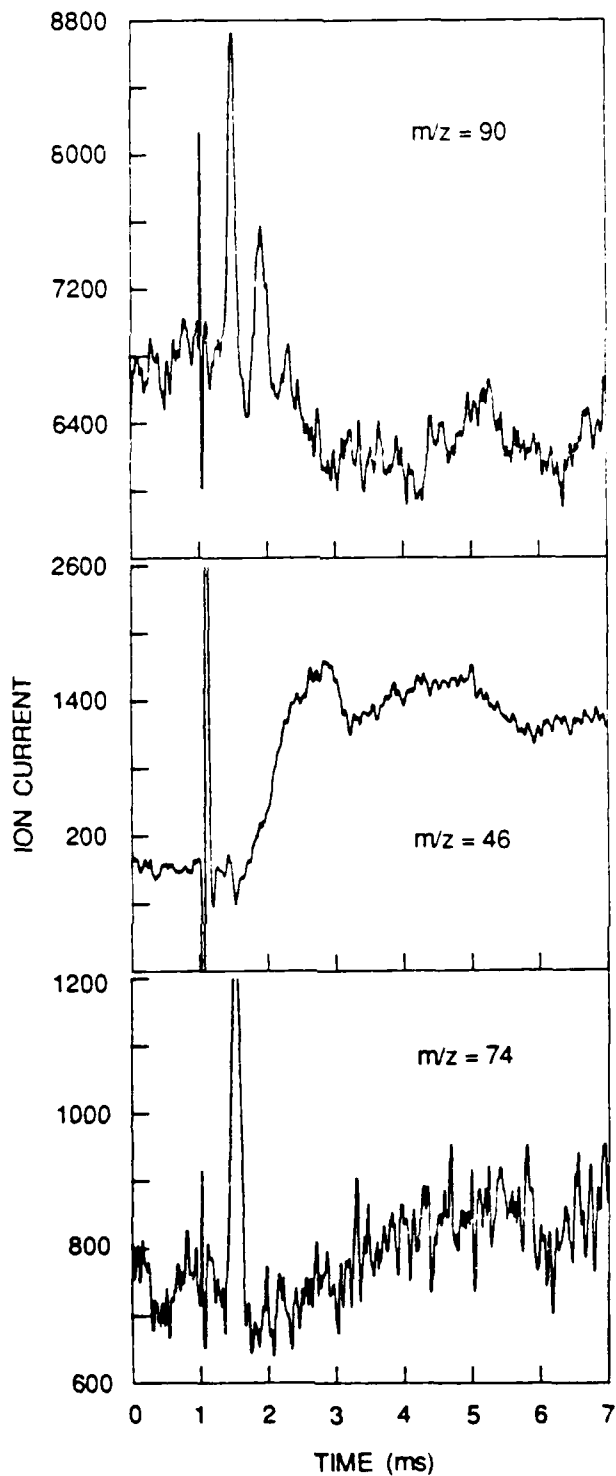
Figure 4. Temporal profiles for m/z 90, 46, and 30.

Changes in m/z 90 are mirrored by m/z 46 and 30. The rise times for m/z 46 and 30 are identical and correspond exactly to the drop in m/z 90 signal.



JA-8232-9

Figure 5. Temporal profiles for m/z 45 and 59.
Both profiles exhibit the same rise time
as m/z 46 and 30.



JA-8232-10

Figure 6. Temporal profiles for m/z 90, 46, and 74.

Obtained under different conditions than those in Figures 3-5. The rise time for m/z 46 corresponds to the fall in m/z 90. However, the rise time for m/z 74 is much slower than for m/z 46 indicating that this species was formed by secondary reactions.

Appendix C

THEORETICAL STUDY OF NITRO-NITRITE REARRANGEMENT OF NH_2NO_2

Roberta P. Saxon and Megumu Yoshimine

(Submitted for publication in J. Phys. Chem., April 1988)

THEORETICAL STUDY OF NITRO-NITRITE REARRANGEMENT OF NH_2NO_2

Roberta P. Saxon
Chemical Physics Laboratory
SRI International
Menlo Park, CA 94025

and

Megumu Yoshimine
IBM Almaden Research Center
San Jose, California 95120-6099

ABSTRACT

Structures of NH_2NO_2 , the four isomers of NH_2ONO , dissociation products, and the transition state for nitro-nitrite rearrangement have been optimized at the MCSCF/4-31G level. The wavefunction of the transition state is characterized by two singly-occupied orbitals. The geometry may be described as separated NH_2 and NO_2 species held together by dipole-dipole interaction. Energies have been obtained by large-scale multireference single and double excitation CI calculations (6-31G* basis). The transition state is predicted to lie 46.68 kcal/m above NH_2NO_2 , 0.87 kcal/m below the $\text{NH}_2 + \text{NO}_2$ asymptote and 26.71 kcal/m above the H-trans, NONO-cis NH_2ONO isomer, to which it leads. From these results, isomerization is expected to be competitive with N- NO_2 bond scission, as observed in recent experiments on thermal decomposition of dimethylnitramine [Stewart, Jeffries, Zellweger, McMillen, and Golden, to be published].

MP 88-096
April 5, 1988

INTRODUCTION

The properties and decomposition kinetics of compounds containing the NO_2 group have been extensively studied both theoretically¹⁻⁸ and experimentally^{3,9-15} in recent years because of the high energy content of such molecules, interest in unimolecular bond cleavage to form radical pairs and the serious theoretical challenges posed by such systems. In particular, a recent experimental investigation¹⁰ of the thermal decomposition of dimethylnitramine (DMNA) $(\text{CH}_3)_2\text{NNO}_2$ has determined the rate constant for DMNA disappearance, $\log k (\text{sec}^{-1}) = 13.5 \pm 0.6 - 37.7 \pm 1.5/2.3\text{RT}$. This temperature dependence is not consistent with the expected primary decomposition process, N- NO_2 bond scission, which has both a larger A factor and a higher activation energy. Numerical modeling satisfactorily reproduces the observed temperature dependence and the observation of high yields of dimethylnitrosamine (DMNO) $(\text{CH}_3)_2\text{NNO}$ as the primary product only when rearrangement to give the nitrite form, $(\text{CH}_3)_2\text{NONO}$ is included as a competitive pathway.

Furthermore, a subsequent experiment¹⁴ in which a molecular beam sampling system was used to examine directly the products of dimethylnitramine decomposition found that the initial products include not only dimethylamino radical, $(\text{CH}_3)_2\text{N}$, and NO_2 , but also comparable amounts of NO and various fragments ions of the nitroxyl radical, $(\text{CH}_3)_2\text{NO}$. The latter two are taken as direct evidence of nitro-nitrite rearrangement since the bond energy to release NO from the nitrite is expected to be small on the basis of calculations^{4,16} and of analogy to known C-ONO compounds.¹⁷

Experimental evidence for nitro-nitrite rearrangement in C-nitro compounds is provided by the work of Wodtke, Hintsa, and Lee¹² who applied

RRKM theory to the data for CH_3NO_2 to estimate a barrier height for isomerization slightly below the bond dissociation energy.

There is, to our knowledge, little theoretical study in the literature of nitro-nitrite rearrangement of nitramines. Melius has reported a barrier³ for rearrangement of NH_2NO_2 but has cautioned¹⁶ that the RHF model used may not be valid for the transition state. For methyl nitrate, McKee³ has optimized a transition state for rearrangement at the HF level, which produces a barrier significantly higher than the bond dissociation energy. He conjectures in this case, as well, that use of a multiconfigurational approach could affect the reported results. Although much of the published, ab initio work on NO_2 -containing molecules has relied on Hartree-Fock-based methods, it has been pointed out^{3,8} that proper description even of the ground state of the stable molecules requires including more than one configuration. The use of a multiconfigurational approach should have an even greater effect on the description of a transition state.

In view of the experimental interest in decomposition of nitramines and evidence for isomerization as well as the lack of multiconfigurational treatments for this important class of compounds, we have undertaken ab initio calculations of nitro-nitrite rearrangement of NH_2NO_2 , the unsubstituted analog of dimethylnitramine. Structures of the stable isomers as well as that of the transition state have been optimized at the MCSCF level using analytic second derivatives. Large-scale configuration interaction (CI) calculations were performed at the optimized geometries for determination of energy differences. In the next section, the design of appropriate MCSCF and subsequent CI calculations is described. Results and discussion are presented in the following section.

CALCULATIONS

Geometries of the stable isomers, the dissociation products, and the transition state have been optimized at the MCSCF level using analytic second derivatives with a standard 4-31G Gaussian basis set.¹⁸ The active space of the MCSCF calculation was carefully chosen to include all the bonds involved in the rearrangement of NH_2NO_2 to NH_2ONO . Following the discussion of Bauschlicher et al.¹⁹ on the design of MCSCF calculations for N_2O_4 , two N-O bonds, two N-O antibonds and analogously, four N-H bonding and anti-bonding orbitals were excluded from the active space. For the NH_2NO_2 isomer, for example, which has the four heavy atoms nearly co-planar, this leads to an eight orbital active space consisting of the four pi orbitals formed from the out-of-plane p's on the heavy atoms and the following four sigma orbitals: two combinations of the in-plane lone pair p orbitals on the O's and the N-N bond and anti-bond pair. The eight orbital MCSCF was used in the geometry optimization of the NH_2NO_2 species. However, for MCSCF calculations on the NH_2ONO isomers, a seven orbital active space converged far more readily. In the calculations on NH_2NO_2 , the lowest-lying orbital in the original active space, one of the oxygen lone pairs, had an occupation number extremely close to 2.0. Therefore, removing this orbital from the active space has essentially no effect on the description of NH_2NO_2 . Geometry optimizations of NH_2ONO and the transition state were performed with the seven orbital active space. Taking all possible distributions of 10 electrons within seven orbitals results in 196 configurations when no symmetry is considered.

Energies were determined by multireference single and double excitation CI calculations with the standard 6-31G* basis set²⁰ using MCSCF molecular orbitals. In constructing the CI expansions, the orbitals were divided into

three spaces, inactive, composed of 4 orbitals, active, composed of 7 orbitals as for the MCSCF, and external. The seven lowest occupied orbitals were kept doubly occupied. For the stable isomers, which have C_s symmetry, test calculations in which the three highest frozen orbitals were transferred to the inactive space were performed. For all CI calculations, the configuration list included all single and double excitations from the inactive and active spaces with at most one electron in the external space and all double excitations from the inactive and active spaces to the external space which differed by no more than two electrons from a set of reference configurations. Interacting space restrictions on the coupling were imposed for double excitations from the inactive space. The weight of the reference configurations in the CI wavefunctions was approximately 0.88 for all calculations. This resulted in CI expansions of ~500,000 to 900,000 configurations in C_s symmetry and 1.8 million in C_1 symmetry. Calculations with the larger inactive space totalled 1 - 1.4 million configurations in C_s symmetry.

Preliminary geometry optimizations were carried out with the GAMESS²¹ program; final geometry determinations and all other calculations used the ALCHEMY II²² program system.

RESULTS AND DISCUSSION

Structures of Stable Isomers

Geometrical parameters for NH_2NO_2 , for the isomers of NH_2ONO and for the stable dissociation products, optimized at the MCSCF level, are given in Tables I-III. There are four isomers of the nitrite depending on whether the hydrogens and the terminal NO are placed cis or trans with respect to the central NO bond. The numbering of the atoms is illustrated in Figure 1. The four heavy atoms of the nitramine are nearly coplanar while the hydrogens are bent with respect to this plane by approximately 15 degrees. For all four isomers of NH_2ONO , the four heavy atoms are strictly coplanar and the hydrogens are symmetric with respect to the plane. There is a double bond between the terminal nitrogen and oxygen with a predicted bond length of 1.6-1.7 Å. NH_2ONO is expected to dissociate readily to $\text{NH}_2\text{O} + \text{NO}$. Comparing 6-31G* MCSCF energies, the maximum energy difference between the isomers is 2.6 kcal/m. Comparing RHF/6-31G* geometries and energies,¹⁶ the isomers are found in a different order in energy, but the maximum spread is similar.

Parameters obtained at the RHF level with the 6-31G* basis as well as those derived from analysis of microwave spectra²³ for NH_2NO_2 are also listed in Table I. A comparison with RHF results with both basis sets is given in Table II for the NH_2ONO isomer which has both the hydrogens and NONO cis. In all cases, qualitatively similar geometries are predicted by both computational models. Examining the MCSCF and RHF parameters obtained with the same basis set in Table II, it is clear that the O1-N2 bond is most dramatically affected by the MCSCF model, lengthening from the RHF prediction of 1.416 Å to the MCSCF value of 1.750 Å. This is consistent with the dominant correlation in the MCSCF wavefunction for NH_2ONO being an excitation to an O1-N2

antibonding orbital. It is possible that the length of the O1-N2 bond is overestimated by the present MCSCF model which does not correlate all bonds to the same extent. A modest difference in geometry due to basis set in calculations at the RHF level is also illustrated in Table II; the 6-31G* bond lengths are all shorter. The maximum difference is 0.07 Å for the O1-N2 bond.

In the nitramine, the MCSCF model has the largest effect on the N-N bond length, which is predicted to be 1.418 Å as compared to 1.356 Å at the RHF/6-31G* level, bringing it into closer agreement with the value, 1.427 Å deduced from experiment. For this case, excitation to the N-N antibonding orbital is an important correlation contribution to the MCSCF wavefunction. In calculations on NH_2NO_2 where all atoms were constrained to be coplanar, MCSCF vs RHF optimization with the 4-31G basis set results in lengthening of the N-N bond by 0.07 Å, from 1.327 Å to 1.400 Å. The total energy is not very sensitive to the location of the hydrogens. The MCSCF energy of the planar species is only 1.6 kcal/m higher than that of the optimized geometry in Table I. The remaining geometrical parameters are in reasonable agreement with those derived from experiment. Note that in the experimental analysis, the four heavy atoms were constrained to be planar and the N-O bond length was assumed. The greatest discrepancy is in the location of the hydrogens. The experimental geometry has them bent from the plane of the heavy atoms by a greater amount and has a somewhat smaller H-N-H bond angle than our calculated values. The geometry of the hydrogens, however, is expected to have little effect on the rearrangement process under investigation here.

Transition State

The geometry of the transition state for rearrangement of NH_2NO_2 to the NH_2ONO (H-trans, NONO-cis) isomer, which is the lowest in energy in these

calculations, is illustrated in Figure 2. The N1, H2, O1, and N2 atoms are nearly coplanar with the O2 above the plane and the H1 extending below the plane. Optimized geometrical parameters are listed in Table IV and calculated harmonic frequencies are given in Table V. This is a true transition state with one imaginary frequency.

The geometry may be described as separated NH_2 and NO_2 species held together by dipole-dipole interaction. The N1-N2 and N1-O1 bonds are extremely long, 2.845 Å and 3.214 Å respectively, and the remaining relevant parameters have almost exactly the values given for the isolated species at the same level of calculation in Table III. The average of the N2-O1 and N2-O2 bond lengths is the same as that in NO_2 with the N2-O1 bond longer by 0.002 Å and the N2-O2 bond correspondingly shorter. As indicated in Table V, all of the significant frequencies correspond strictly to internal motion of one fragment or the other. Motions connecting the two halves of the molecule have extremely low frequencies. As would be expected for this loose combination of two radical species, the MCSCF wavefunction for the transition state is characterized by two singly occupied orbitals. This transition state could not have been located by a Hartree-Fock based method.

The geometry reported in Table IV is identified as a transition state by the calculation of all zero gradients and one negative second derivative. The calculations illustrated in Figure 3 verify that this transition state does in fact connect the NH_2NO_2 and NH_2ONO (H-trans, NONO-cis) species, as claimed. The N1-N2 bond distance is taken as the reaction coordinate for the left half of the plot describing the path between NH_2NO_2 and the transition state. Fixing the N1-N2 bond length at particular distances between the value for NH_2NO_2 and the transition state, the remaining geometrical parameters were optimized at the MCSCF/4-31G level. The relative energies shown in Figure 3

were obtained by subsequent MCSCF calculations with the 6-31G* basis. Analogous calculations were performed for the path between the transition state and the nitrite using the N1-O1 bond length as the reaction coordinate. The transition state is found to be the highest energy point between NH_2NO_2 and the H-trans, NONO-cis nitrite isomer and to connect smoothly to both forms. It does not, however, lead to the H-trans, NONO-trans NH_2ONO isomer. The barrier to formation of that isomer is calculated (MCSCF/4-31G) to be 15 kcal/m higher than the transition state. (We have considered only NH_2ONO isomers with the H's trans because they are approximately trans in the transition state.)

Energies

Test calculations probing the effect of the size of the inactive space in the CI expansion were performed taking advantage of the C_s symmetry of the stable species. The energy difference between one of the NH_2ONO isomers (H-trans, NONO-trans) and NH_2NO_2 obtained with the seven orbital inactive space (denoted CI7) is compared with that from the four orbital inactive space (CI4) in Table VI. The Davidson correction²⁴ for the effect of quadruple excitations, also listed in Table VI, should provide a reasonable estimate in these calculations because the weight of the reference configurations is very similar in all of the wavefunctions. The energy difference of 21.39 kcal/m obtained from the CI4 calculations with the Davidson correction is in reasonable agreement with the value of 19.04 kcal/m from the larger CI, justifying the use of the four orbital inactive space for the transition state for which there is no symmetry to reduce the size of the CI expansion.

A comparison between the energy difference at the MCSCF/4-31G and RHF/6-31G* optimized geometries is also provided in Table VI. At the same

level of calculation (CI7), the difference in energy difference due to geometry is only 1 kcal/m. In addition, at the RHF geometry, we compare the energy difference from the present CI calculations to that previously obtained with a perturbation-theory approach (MP4/6-31G^{**}). For these closed-shell isomers, a difference in prediction of 3.5 kcal/m is found.

The final results of our study are presented in Table VII which lists CI energies for the transition state, the $\text{NH}_2 + \text{NO}_2$ asymptote, and the NH_2ONO (H-trans, NONO-cis) isomer to which the transition state leads, at MCSCF/4-31G optimized geometries. The transition state is predicted to lie 46.68 kcal/m above NH_2NO_2 , 0.87 kcal/m below the asymptote and 26.71 kcal/m above the H-trans, NONO-cis nitrite isomer.

Discussion

In the following discussion, we assume the results obtained here for the unsubstituted nitramine can be applied directly to dimethylnitramine which has been studied experimentally. This appears to be a reasonable assumption for isomerization and bond dissociation in that the hydrogens remain as spectators in both processes. Because the frequencies of the transition state are very similar to those of the separated products, consideration of zero point energy will not affect the conclusion that within the uncertainty of the calculation, the barrier to nitro-nitrite rearrangement is the same as the energy to break the N- NO_2 bond. Furthermore, the A factors for isomerization and bond scission should also be quite similar, leading to the prediction that the two paths should compete quite evenly. This in agreement with the conclusion from the molecular-beam-sampled experiment¹⁴ on DMNA that the rearrangement/N- NO_2 bond scission branching ratio (at ca. 900K) is ~0.7. While the present results are in qualitative agreement with the inference of the importance of

nitro-nitrite rearrangement in explaining the observed temperature dependence in the earlier decomposition study,¹⁰ they do not support the assumption of a small A factor and of an isomerization barrier 15 kcal/m below the bond dissociation energy required by the kinetic model.

With respect to the computational model, our results indicate the MCSCF approach is essential to determining the open-shell transition state for nitro-nitrite rearrangement. The closed shell prediction for the transition state using the RHF model¹⁶ is characterized by much shorter bond lengths and is significantly higher in energy than the transition state reported here. Optimization of the stable isomers at the MCSCF level, understandably, has the greatest effect on the bond being correlated in the MCSCF. This effect appears to be comparable, for example, in NH_2NO_2 and in NH_2ONO leading to a similar energy difference between isomers for the MCSCF- and RHF-optimized geometries. Application of this MCSCF model to additional N-nitro and C-nitro compounds should lead to interesting results.

ACKNOWLEDGMENTS

The authors gratefully acknowledge informative conversations with Dr. Carl Melius and extensive communication of unpublished results. Receipt of unpublished results from Dr. Steve Rogers and Dr. Donald Thompson is also appreciated. RPS supported by AFOSR under contract No. F49620-85-K-00006. Work performed under joint study agreement between SRI and IBM.

REFERENCES

1. M.J.S. Dewar, J. P. Ritchie, and J. Alster, *J. Org. Chem.* 50, 1031 (1985).
2. A. G. Turner and L. P. Davis, *J. Am. Chem. Soc.* 106, 5447 (1984).
3. M. L. McKee, *J. Am. Chem. Soc.* 108, 5784 (1986) and references quoted therein.
4. C. F. Melius and J. S. Binkley, "Thermochemistry of the Decomposition of Nitramines in the Gas Phase," 21st International Symposium on Combustion, Munich, Germany (August 1986).
5. S. R gers, personal communication.
6. B. G. Sumpter and D. L. Thompson, *J. Chem. Phys.* 86, 3301 (1987).
7. J. P. Ritchie, *J. Am. Chem. Soc.* 107, 1829 (1985).
8. D. S. Marynick, A. K. Ray, and J. L. Fry, *Chem. Phys. Lett.* 116, 429 (1985).
9. A. C. Gonzalez, C. W. Larson, D. F. McMillen, and D. M. Golden, *J. Phys. Chem.* 89, 4809 (1985).

10. S. E. Nigenda, D. F. McMillen, and D. M. Golden, to be published, J. Phys. Chem. (1988).
11. S. A. Lloyd, M. E. Umstead, and M. E. Lin, J. Energetic Materials 3, 187 (1985).
12. A. M. Wodtke, E. J. Hintsa, and Y. T. Lee, J. Phys. Chem. 90, 3549 (1986).
13. X. Zhao, E. J. Hintsa, and Y. T. Lee, J. Chem. Phys. 88, 801 (1988).
14. P. H. Stewart, J. B. Jeffries, J.-M. Zellweger, D. M. Golden, and D. F. McMillen, to be published.
15. M. A. Schroeder, "Critical Analysis of Nitramine Decomposition Results: Some Comments on Chemical Mechanisms," Proc. 16th JANNAF Comb. Mtg., CPIA, 1978, 82, 644 14 September, 1979, Vol. 2, p. 17.
16. C. F. Melius, personal communication.
17. L. Batt and G. N. Robinson, "Thermochemistry of Nitro Compounds, Amines, and Nitroso Compounds," in Chemistry of Functional Groups: Supplement F, Ed., S. Patai, J. Wiley and Sons, Ltd., Chichester, p. 1035 (1981).
18. R. Ditchfield, W. J. Hehre, and J. A. Pople, J. Chem. Phys. 54, 724 (1971).

19. C. W. Bauschlicher, A. Komornicki, and B. Roos, *J. Am. Chem. Soc.* 105, 745 (1983).
20. P. C. Hariharan and J. A. Pople, *Theor. Chim. Acta* 28, 213 (1973).
21. M. Dupuis, J. J. Wendoloski, and D. Spangler, *D. Natl. Res. Comput. Chem. Software Cat.* 1, QG01 (1980).
22. B. H. Lengsfeld, III, *J. Chem. Phys.* 73, 382 (1980); B. H. Lengsfeld and B. Liu, *J. Chem. Phys.* 75, 478 (1981); B. Liu and M. Yoshimine, *J. Chem. Phys.* 74, 612 (1981).
23. J. K. Tyler, *J. Mol. Spectrosc.* 11, 39 (1963).
24. S. R. Langhoff and E. R. Davidson, *Int. J. Quantum Chem.* 8, 61 (1974).

Table I. Optimized geometrical parameters for NH_2NO_2
in Angstroms and degrees.

	<u>MCSCF/4-31G^a</u>	<u>RHF/6-31G^{*b}</u>	<u>Experiment^c</u>
N1-N2	1.418	1.356	1.427±0.002
N2-O1	1.227	1.191	1.206 (assumed)
N1-H	0.991	0.998	1.005±0.010
<H-N-H	123.3	116.8	115.2±2.
<O1-N2-O2	126.6	127.0	130.1±0.3
<H-N1-N2	113.8	110.5	
<N1-N2-O	116.7	116.5	
<O2-N2-O1-N1 ^d	178.1	177.6	180.0
<H1-N1-N2-O1 ^d	16.8	25.6	
<H2-N1-N2-O1 ^d	164.9	156.5	
energy (hartrees)			
MCSCF/6-31G [*]	-259.71268	-259.71665	

^aEight orbital active space, including one additional O lone pair orbital, was used for this optimization.

^bC. Melius, Ref. 16.

^cJ. K. Tyler, Ref. 23. Angle between NH_2 and NNO_2 plane = 51.8±1.

^dTorsion angles.

Table II. Optimized geometrical parameters of NH₂ONO isomers in Angstroms and degrees.

	H-cis ^a NONO-cis			H-cis NONO-trans
	<u>MCSCF/4-31G</u>	<u>RHF/4-31G</u>	<u>RHF/6-31G^{*b}</u>	<u>MCSCF/4-31G</u>
	N1-O1	1.384	1.418	1.391
O1-N2	1.750	1.416	1.342	1.720
N2-O2	1.167	1.171	1.159	1.164
N1-H	0.994	0.997	1.003	0.995
<H-N1-O1	113.2	110.2	107.0	111.2
<N1-O1-N2	109.9	117.1	117.5	108.0
<O1-N2-O2	110.8	114.7	115.3	109.6
<H1-N1-H2	117.0	114.8		115.6
<H-N1-O1-N2 ^c	68.1	63.8	57.4	65.2
<O2-N2-O1-N2 ^c	0.0	0.0	0.0	180.0
energy (hartrees)				
MCSCF/6-31G [*]	-259.70284			-259.70225
relative energy ^d (kcal/m)				
	2.3			2.6
	H-trans NONO-cis		H-trans NONO-trans	
	<u>MCSCF/4-31G</u>		<u>MCSCF/4-31G</u>	<u>RHF/6-31G^{*b}</u>
N1-O1	1.403		1.413	1.393
O1-N2	1.714		1.675	1.356
N2-O2	1.159		1.164	1.153
N1-H	0.996		0.996	1.002
<H-N1-O1	109.5		108.1	104.5
<N1-O1-N2	107.6		105.5	108.7
<O1-N2-O2	113.0		109.1	110.2
<H1-N1-H2	115.2		114.3	
<H-N1-O1-N2 ^c	116.4		117.9	123.5
<O2-N2-O1-N2 ^c	0.0		180.0	180.0
energy (hartrees)				
MCSCF/6-31G [*]	-259.70644		-259.70584	
relative energy				
(kcal/m)	0.0		0.4	

^aOrientation of H's with respect to N1-O1 bond.

^bC. Melius, Ref. 16.

^cTorsion angles.

^dWith respect to H-trans NONO cis.

Table III. Optimized geometrical parameters for dissociation products
in Angstroms and degrees (MCSCF/4-31G)

<u>NH₂</u>		<u>NO₂</u>	
N-H	1.014	N-O	1.210
<H-N-H	108.4	<O-N-O	133.1

Table IV. Optimized geometrical parameters for $\text{NH}_2\text{NO}_2 \rightarrow \text{NH}_2\text{ONO}$ transition state in Angstroms and degrees (MCSCF/4-31G).

N1-N2	2.845
N1-O1	3.214
N2-O1	1.212
N2-O2	1.207
N1-H	1.014
<O1-N2-O1	133.1
<H2-N1-H1	108.3
<H2-N1-N2	96.3
<H1-N1-N2	110.3
<N1-N2-O1	96.4
<N1-N2-O2	111.1
<O2-N2-O1-N1 ^a	126.9
<H1-N1-N2-O1 ^a	102.5
<H2-N1-N2-O1 ^a	9.7

^aTorsion angle.

Table V. $\text{NH}_2\text{NO}_2 \rightarrow \text{NH}_2\text{ONO}$ Transition State Frequencies (cm^{-1})
(MCSCF/4-31G)

<u>NO₂</u> Expt ^a	<u>Transition State</u>	<u>NH₂</u> calculation	
		b	c
Imaginary	(184.7)		
	43.7		
	67.7		
	91.0		
	173.7		
	294.1		
749.8	752.7 ^d		
1319.7	1324.4 ^d		
	1668.9 ^e	1527.6	1540
1617.75	1728.0 ^d		
	3545.4 ^e	3221.4	3307
	3664.1 ^e	3311.2	3627

^aG. Herzberg, "Electronic Spectra of Polyatomic Molecules," (Van Nostrand, New York, 1966).

^bC. Melius, Ref. 16.

^cR. J. Buenker, M. Peric, S. D. Peyerimhoff, and R. Marian, Mol. Phys. 43, 987 (1981).

^dPure NO₂ motion.

^ePure NH₂ motion.

Table VI. Energy differences between NH_2NO_2 and NH_2ONO (H-trans, NONO-trans) 6-31G* basis except as noted.

	NH_2NO_2	NH_2ONO	
		H-trans NONO-trans	
	total energy	total energy	
	(hartrees) ^a	(hartrees) ^a	ΔE (kcal/m)
<u>MCSCF/4-31G Geometry</u>			
MCSCF	-0.712682	-0.705836	4.30
CI7 ^b	-1.283697 ^c	-1.253592 ^d	18.90
CI7D ^e	-1.360033	-1.329993	19.04
CI4 ^b	-1.29359 ^c	-1.096175 ^d	20.83
CI4D ^e	-1.177215	-1.143141	21.39
<u>RHF/6-31G* Geometry</u>			
MCSCF	-0.716648	-0.707247	5.90
CI7	-1.284231	-1.256609	17.34
CI7D	-1.357619	-1.328820	18.08
RHF ^f	-0.647174	-0.615038	20.17
MP4 ^f	-0.386522	-0.352174	21.56

^aWith respect to -259.0 hartrees.

^bCI7 (CI4) denotes CI with 7 (4) orbital inactive space (see text).

^c NH_2NO_2 C_s symmetry CI7: 1,080,501 configurations
CI4: 597,551 configurations

^d NH_2ONO C_s symmetry CI7: 1,445,944 configurations
CI4: 816,400 configurations

^eCI7D (CI4D) denotes CI7 (CI4) with Davidson correction for quadruple excitations.

^f6-31G** basis set. C. Melius, Ref. 16.

Table VII. Total energy of transition state, asymptote,
and NH_2ONO (H-trans, NONO-cis)
(6-31G* basis set, MCSCF/4-31G optimized geometry).

	Transition State		$\text{NH}_2 + \text{NO}_2$		NH_2ONO (H-trans NONO-cis)	
	total energy ^a (hartrees)	energy above NH_2NO_2 (kcal/m)	total energy ^a (hartrees)	energy above NH_2NO_2 (kcal/m)	total energy ^a (hartrees)	energy above NH_2NO_2 (kcal/m)
MCSCF	-0.658889	33.77	-0.656990	34.96	-0.706436	3.92
CI4 ^b	-1.050382	49.57	-1.049494	50.13	-1.098305	19.49
CI4D ^b	-1.102852	46.68	-1.101460	47.55	-1.145406	19.97

^aWith respect to -259.0 hartrees.

^bDefined in Table VI.

FIGURE CAPTIONS

- Figure 1. MCSCF/4-31G optimized equilibrium geometry of NH_2NO_2 and two NH_2ONO isomers. (a) N1, N2, O1, O2 are nearly co-planar. (b) cis and trans are designated with respect to N1-O1 bond. N1, N2, O1, O2 are strictly coplanar and bisect $\angle \text{H1N1H2}$.
- Figure 2. MCSCF/4-31G optimized transition state for rearrangement of NH_2NO_2 to NH_2ONO (H-trans, NONO-cis).
- Figure 3. Energy (kcal/m) with respect to NH_2NO_2 (MCSCF/6-31G^{*}) for path connecting NH_2NO_2 , transition state, and NH_2ONO (H-trans, NONO-cis). Left side: For fixed N1-N2 bond length as the reaction coordinate, all other geometrical parameters were optimized. Right side: N1-O1 taken as reaction coordinate.

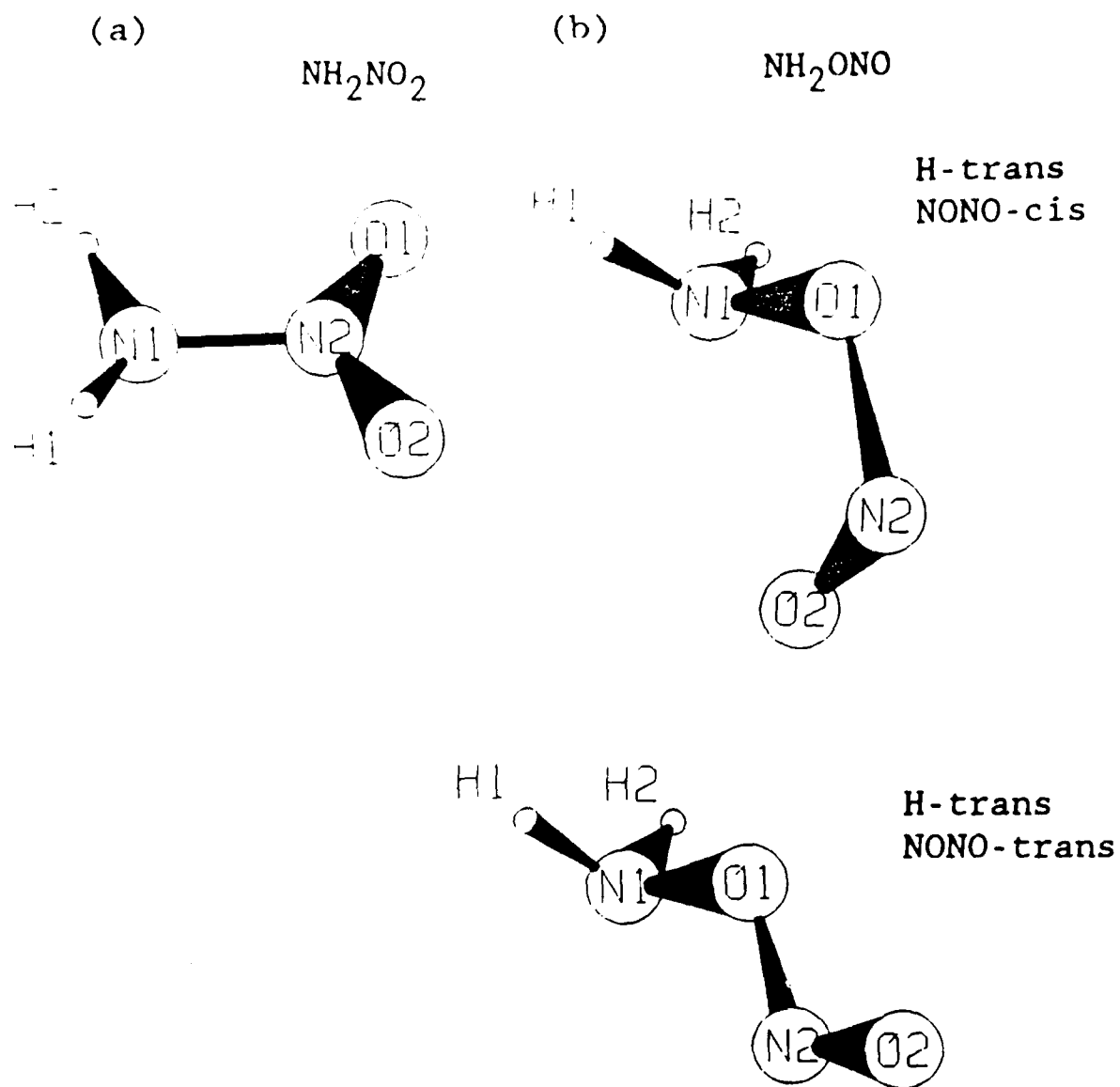


Figure 1. MCSCF/4-31G optimized equilibrium geometry of NH_2NO_2 and two NH_2ONO isomers. (a) N1, N2, O1, O2 are nearly co-planar. (b) cis and trans are designated with respect to N1-O1 bond. N1, N2, O1, O2 are strictly coplanar and bisect $\angle \text{H1N1H2}$.

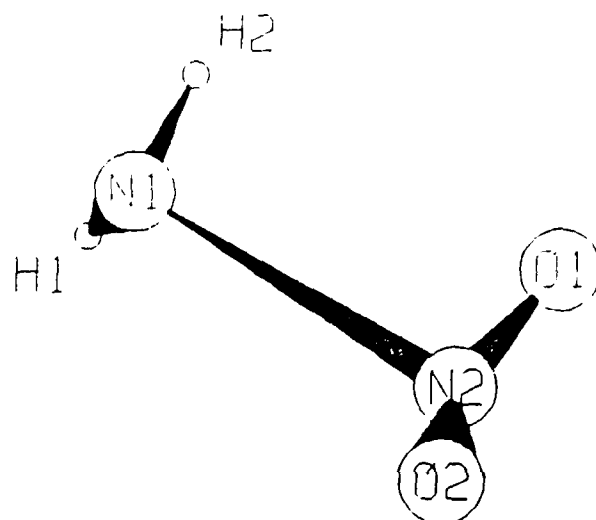


Figure 2. MCSCF/4-31G optimized transition state for rearrangement of NH_2NO_2 to NH_2ONO (H-trans, NONO-cis).

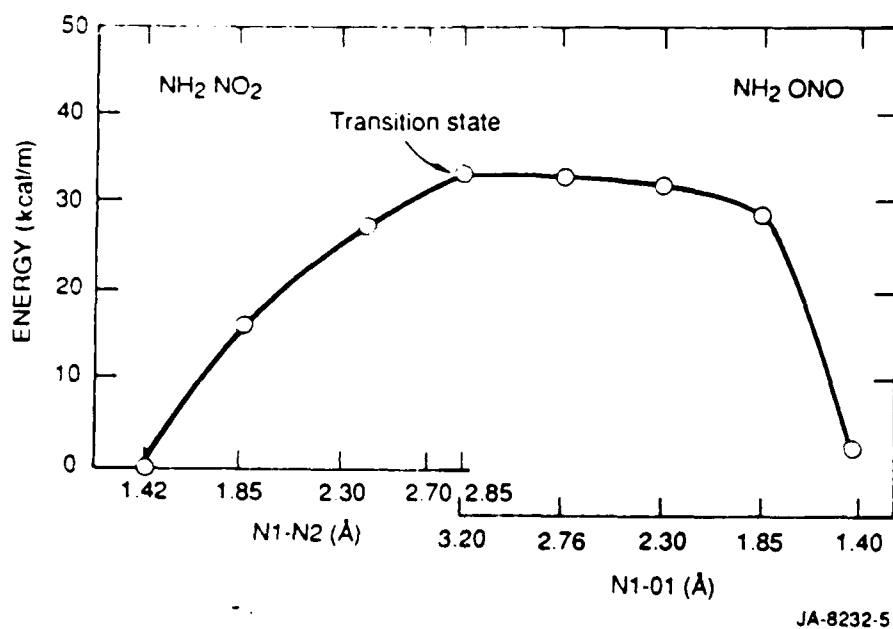


Figure 3. Energy (kcal/m) with respect to NH_2NO_2 (MCSCF/6-31G^{*}) for path connecting NH_2NO_2 , transition state, and NH_2ONO (H-trans, NONO-cis). Left side: For fixed N1-N2 bond length as the reaction coordinate, all other geometrical parameters were optimized. Right side: N1-O1 taken as reaction coordinate.

Appendix D

SYNTHESIS OF N,N-DIMETHYLNITRAMINE BY
NITRODEPHOSPHORYLATION OF HEXAMETHYLPHOSPHORAMIDE

Jeffrey C. Bottaro, Clifford D. Bedford,
Robert J. Schmitt, and Donald F. McMillen

(Submitted for publication in J. Org. Chem., March 1988)

SYNTHESIS OF N,N-DIMETHYLNITRAMINE BY
NITRODEPHOSPHORYLATION OF HEXAMETHYLPHOSPHORAMIDE

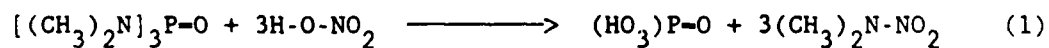
Jeffrey C. Bottaro,* Clifford D. Bedford,
Robert J. Schmitt, and Donald F. McMillen

Energetic Materials Program, SRI International
333 Ravenswood Avenue, Menlo Park, CA 94025, USA.

ABSTRACT: Addition of hexamethylphosphoramide to anhydrous nitric acid at 0° to 10°C gives a 200% yield of N,N-dimethylnitramine, along with a 12% yield of N,N-dimethylnitrosamine, based on hexamethylphosphoramide.

Sir:

The large-scale synthesis of N,N-dimethylnitramine^{1,2} poses serious safety problems resulting primarily from the formation of nitrosamine by-product and the use of potentially explosive mixtures of nitric acid and acetic or trifluoroacetic anhydride.^{3,4} In our search for a safe, pilot-plant-scale synthesis of this material (not currently available commercially), we examined the ostensibly exothermic metathesis of a phosphoryl amine with nitric acid--in this case hexamethylphosphoramide (HMPA)--to give dimethylnitramine and phosphoric acid.



This synthesis has proved viable in practice. We isolated a 200% yield of N,N-dimethylnitramine and only a small amount (12%) of the carcinogenic N,N-dimethylnitrosamine impurity when the reaction was run on roughly a half-mole scale, based on starting HMPA. The reaction was run between 0° and 10°C; ice-bath cooling was required. The products were isolated by neutralization with cooling, followed by chloroform extraction.

Notably, only two of the three dimethylamino ligands underwent nitration to give a 200% yield, rather than all three giving the maximum possible 300% yield of the desired product. Further study will reveal the fate of the currently unaccounted-for dimethylamino ligand.

The implications of this observation for explosive technology are significant. A phosphorus-based scaffold might be feasible as an incipient polynitramine framework, using variations on the reaction described here. Elaborations of this methodology are being investigated.

EXPERIMENTAL

Caution! This procedure produces traces of N,N-dimethylnitrosamine, a known carcinogen.

Hexamethyl phosphoramidate (50 g, 0.28 mole) was added dropwise to a stirred mass of 600 g (400 mL) of 100% nitric acid in a 1-L flask cooled by an ice-bath. The rate of addition was carefully regulated to prevent the reaction mixture from ever heating beyond 10°C; the addition time was approximately 90 min. After the addition was complete, the reaction

mixture was allowed to warm to room temperature over an additional 90 min. Workup was carried out by quenching the reaction mixture into 1 kg of ice, neutralizing with 400 g of NaOH with ice-cooling of the diluted mixture, and extracting with 3 x 200 mL of chloroform. Drying, filtering, and concentrating, followed by crystallization from carbon tetrachloride, gave 50 g (200%) of N,N-dimethylnitramine, mp 53-55°C. The mother liquor yielded 3 g (12%) of dimethylnitrosamine, a yellow liquid with nonequivalent methyls in its NMR spectrum.

References

1. John H. Robson and Joan Reinhart, J. Am. Chem. Soc. 1955, 77, 2453.
2. John H. Robson and Joan Reinhart, J. Am. Chem. Soc. 1955, 77, 107.
3. C. D. Bedford, Chem. Eng. News, 1980, 58(35), 33, 43.
4. C. Coon, Lawrence Livermore National Laboratory, 1987 (Personal Communication).

Acknowledgement:

We wish to thank the Army Research Office (Contract No. DAAC03-86-K-0030) and the Air Force Office of Scientific Research (Contract No. F49620-85-K-00006) for support of this research.